

OPEN ACCESS

## Review—Conversion Coatings Based on Zirconium and/or Titanium

To cite this article: I. Milošev and G. S. Frankel 2018 *J. Electrochem. Soc.* **165** C127

View the [article online](#) for updates and enhancements.

### You may also like

- [Nano  \$\text{Al}\_2\text{O}\_3\$ /phosphate Composite Conversion Coating Formed on Magnesium Alloy for Enhancing Corrosion Resistance](#)  
Ming Zhao, Jianguo Li, Guangping He et al.
- [Nano ZnO-assisted formation of zinc phosphate conversion coating for improving corrosion protection of AZ91D magnesium alloy](#)  
Gui Lou, Peng Jia, Xinying Teng et al.
- [Comparison of the Electrochemical Behaviour and Self-sealing of Zirconium Conversion Coatings Applied on Aluminium Alloys of series 1xxx to 7xxx](#)  
Gavriilo Šekularac, Janez Kova and Ingrid Milošev

## PAT-Tester-x-8 Potentiostat: Modular Solution for Electrochemical Testing!

**EL-CELL®**  
electrochemical test equipment

- ✓ **Flexible Setup with up to 8 Independent Test Channels!**  
Each with a fully equipped Potentiostat, Galvanostat and EIS!
- ✓ **Perfect Choice for Small-Scale and Special Purpose Testing!**  
Suited for all 3-electrode, optical, dilatometry or force test cells from EL-CELL.
- ✓ **Complete Solution with Extensive Software!**  
Plan, conduct and analyze experiments with EL-Software.
- ✓ **Small Footprint, Easy to Setup and Operate!**  
Usable inside a glove box. Full multi-user, multi-device control via LAN.



Contact us:

+49 40 79012-734

[sales@el-cell.com](mailto:sales@el-cell.com)

[www.el-cell.com](http://www.el-cell.com)



## Review—Conversion Coatings Based on Zirconium and/or Titanium

I. Milošev<sup>1,\*</sup> and G. S. Frankel<sup>2,\*\*</sup>

<sup>1</sup>Department of Physical and Organic Chemistry, Jožef Stefan Institute, SI-1000 Ljubljana, Slovenia

<sup>2</sup>Fontana Corrosion Center, The Ohio State University, Columbus, Ohio 43210, USA

There is a growing interest in conversion coatings based on titanium and/or zirconium as the result of the health and environmental issues associated with legacy chromate and phosphate conversion coatings. Any alternative technology should be environmentally friendly and cost effective, and also able to achieve comparable corrosion resistance and paint adhesion for ferrous and non-ferrous substrates. Conversion coatings based on titanium or zirconium seem to fulfill many of these requirements and thus offer a great potential for further applications. This literature review summarizes the scientific results in this rapidly growing area of research. Following the description of composition of conversion bath and deposition mechanism, the effects of process parameters for conversion baths such as pH, temperature, immersion time and agitation are presented together with coating characteristics. The effects of the type of substrate and substrate pre-treatment are explored for the most-studied substrates: Al alloys, zinc-coated steels and steels. Properties such as composition, morphology and thickness are summarized. The corrosion performance of the conversion coatings is discussed, as well as adhesion of organic coatings and delamination mechanism for a full coating system including substrate/coating/top-coat.

© The Author(s) 2018. Published by ECS. This is an open access article distributed under the terms of the Creative Commons Attribution 4.0 License (CC BY, <http://creativecommons.org/licenses/by/4.0/>), which permits unrestricted reuse of the work in any medium, provided the original work is properly cited. [DOI: 10.1149/2.0371803jes]



Manuscript submitted October 16, 2017; revised manuscript received February 1, 2018. Published February 17, 2018.

Metals used in the construction of products and facilities in most applications, including industrial, infrastructure, transportation, construction, consumer goods, etc., are primarily selected from three groups: steels, zinc-coated (galvanized) steels, and aluminum alloys (AA).<sup>1</sup> All of these materials require protection to prevent environmental degradation, and the most common approach to protection against corrosion is a multilayer coating system. Metal components are treated by a series of processes to create this coating system: cleaning, surface pre-treatment, and application of organic coating layers including primer and topcoat. Surface pre-treatments include anodizing (for aluminum alloys) and conversion coatings, which are the focus of this review. Conversion coatings are formed by immersion of a component in a chemical bath and reaction of the metal substrate with the components in the bath to form a layer that coats the surface. These layers provide some corrosion protection by acting as a barrier to the environment or releasing corrosion-inhibiting species. However, their primary role is to improve the adhesion of subsequently applied paint layers.

The most important conversion coatings used for corrosion protection and adhesion promotion of ferrous and non-ferrous metal substrates are chromate conversion coatings (CCCs) and phosphate coatings. CCCs are highly corrosion protective. They consist of a backbone of chromium oxide/hydroxide with Cr in the 3+ oxidation state and also contain compounds with Cr in the 6+ oxidation state.<sup>2-5</sup> The Cr(VI) provides the characteristic of self-healing, which is the ability to reform a protective coating after it has been breached by a mechanical or chemical process. Self-healing in CCCs occurs by the reduction of remaining Cr(VI) in the coating to an insoluble Cr<sup>3+</sup> compound. Phosphate coatings are hard, continuous, insoluble and electrically non-conducting and are used in numerous applications in the automotive, agriculture and appliance industries.<sup>6</sup>

Both CCCs and phosphating have some health, environmental and energy drawbacks. Chromate compounds are toxic and carcinogenic. Their use presents health hazard for workers and requires costly monitoring and disposal.<sup>7</sup> The use of hexavalent chromium is restricted in the European Union and the USA.<sup>8,9</sup> Phosphate coatings cause different problems; discharge from concentrated phosphate baths has a detrimental effect on groundwater sources due to eutrophication in fresh water lakes and reservoirs.<sup>10</sup> Therefore, use of phosphorus is also restricted by environmental regulations.<sup>8,10</sup> Furthermore, phosphating

baths operate above room temperature, from 30 to 99°C, typically about 50°C, which requires energy input.<sup>11</sup> Finally, phosphating baths generate a large amount of sludge containing metal ions, which necessitates frequent desludging to maintain optimum bath operation. As a result of these issues, phosphate conversion coatings are being increasingly replaced and alternatives are being continuously sought.

The environmental legislation and health concerns have motivated a large number of studies devoted to potential alternatives for chromate and phosphate technology over the last two decades. The goal is to find a technology that would be ecologically acceptable, harmless for human health, operate at lower energy costs, produce less discharge with low amount of heavy or regulated metal ions (Zn, Ni, Mn) and yet achieve comparable effectiveness in terms of corrosion resistance and paint adhesion for ferrous and non-ferrous metal substrates. These demands are not easy to achieve and potential alternatives investigated in the literature comprise a large variety of chemistries including molybdate, permanganate, refractory metal oxyfluorides, phosphates, plasma coatings, sol-gel coatings, self-assembling layers, conducting polymers, inhibitors, hydrotalcites, rare earth coatings, and conversion coatings based on titanium and/or zirconium, as addressed in several review papers.<sup>12-18</sup> Only a few of the investigated systems have reached the maturity of final commercial utilization in industry, and the most important are the conversion coatings based on titanium and/or zirconium, which are the subject of the present review.

In the late 1980s and 1990s, several patents<sup>19-21</sup> were published describing the deposition of Ti and Zr based conversion coatings from hexafluoro-titanate and -zirconate solutions, and these have led to commercial products. The processes of conversion and deposition from these baths are fast, they contain no or small amounts of phosphate or heavy metals, and the coatings are thin and usually colorless. Aluminum and aluminum alloy substrates have been a constant focus of these studies with the aim of replacing legacy chromate or phosphate coatings. Between 2005 and 2015 the interest in galvanized steel substrates intensified. In last few years the focus seems to be directed to the protection of steels, and the number of related studies almost reached that on Al alloys. Based on numerous patents, e.g.<sup>22-26</sup> the first generation of Zr conversion coatings was introduced to the automobile industry in 2005.<sup>27,28</sup> The Ti and Zr coatings are significantly thinner than CCCs and, especially, phosphate coatings. Significant operational cost savings (30%) have been realized without sacrificing corrosion resistance or paint adhesion compared to zinc phosphate coatings.<sup>28</sup> The performance of the first generation was comparable for non-ferrous metal substrates but not for ferrous materials, i.e. cold-rolled steel. The second generation of Zr coatings, being 2.5 x thicker

\*Electrochemical Society Member.

\*\*Electrochemical Society Fellow.

<sup>†</sup>E-mail: [ingrid.milosev@ijs.si](mailto:ingrid.milosev@ijs.si)

**Table I. Non-commercial Ti-, Ti/Zr- and Zr-based coatings on different substrates.**

Conversion bath	Substrate	Reference
<b>Ti-based coatings</b>		
H <sub>2</sub> TiF <sub>6</sub>	Al alloys	41,42,44,77,110
H <sub>2</sub> TiF <sub>6</sub>	Mg alloys	38,71
H <sub>2</sub> TiF <sub>6</sub>	Zn-coated steels	31,41,54,72
K <sub>2</sub> TiF <sub>6</sub>	Zn-coated steels	32
TiCl <sub>3</sub> + H <sub>2</sub> SiF <sub>6</sub>	Zn-coated steels	79
TiCl <sub>4</sub> + H <sub>2</sub> SiF <sub>6</sub>	Zn-coated steels	35
H <sub>2</sub> TiF <sub>6</sub>	Steels	66,73
TiCl <sub>4</sub>	Steels	73,82
<b>Mixed Zr/Ti coatings</b>		
H <sub>2</sub> TiF <sub>6</sub> + H <sub>2</sub> ZrF <sub>6</sub>	Al alloys	19,29,50,59,61,107,136
K <sub>2</sub> TiF <sub>6</sub> + K <sub>2</sub> ZrF <sub>6</sub>	Al alloys	74
H <sub>2</sub> TiF <sub>6</sub> + H <sub>2</sub> ZrF <sub>6</sub>	Mg alloys	60
K <sub>2</sub> ZrF <sub>6</sub> + tetra-n-butyl titanate	Mg alloys	69,70,137
H <sub>2</sub> TiF <sub>6</sub> + H <sub>2</sub> ZrF <sub>6</sub>	Zn-coated steel	48,54
<b>Zr-based coatings</b>		
H <sub>2</sub> ZrF <sub>6</sub>	Al alloys	41,47,49,53,58,64
K <sub>2</sub> ZrF <sub>6</sub>	Al alloys	30
K <sub>2</sub> ZrF <sub>6</sub> + Cr <sub>2</sub> (SO <sub>4</sub> ) <sub>3</sub>	Al alloys	75
Zr(NO <sub>3</sub> ) <sub>4</sub> + NaF	Al	33
ZrO(NO <sub>3</sub> ) <sub>3</sub> + H <sub>2</sub> O <sub>2</sub>	Al alloys	81
H <sub>2</sub> ZrF <sub>6</sub>	Mg alloys	38,71
K <sub>2</sub> ZrF <sub>6</sub>	Mg alloys	36,37
ZrOCl <sub>2</sub>	Mg alloys	80
H <sub>2</sub> ZrF <sub>6</sub>	Zn and Zn-coated steels	41,51,52,55,78
H <sub>2</sub> ZrF <sub>6</sub>	Steels	57,65,67,125,138
Ammonium Zr carbonate	Steels	119

than the first generation, was introduced in 2010 and also achieved comparable performance for cold-rolled steel substrates.<sup>28</sup>

The review is organized into ten subsections. Following the description of the composition of conversion baths and a general deposition mechanism, the process parameters for conversion baths, i.e. pH, temperature, immersion time and agitation, are presented together with their effects on coating characteristics. The effect of substrate on the coating formation is explored for the three most investigated substrates: Al alloys, galvanized steel and steels. Substrate pre-treatment and surface chemistry are critical parameters in the conversion and deposition processes. Characteristics of conversion coatings are described, including composition, morphology and thickness. Corrosion performance of conversion coating is discussed for each type of substrate individually, as well as adhesion of organic coatings and delamination mechanism when fully coated (substrate/coating/top-coat). This literature review primarily considers published scientific results with the aim to review hitherto collected data and knowledge and to point out issues that need further investigation. Advantages and potential drawbacks are present in the last section.

### Composition of Zr- and Ti-Based Conversion Baths

A typical Zr or Ti conversion bath contains hexafluoro zirconic acid, H<sub>2</sub>ZrF<sub>6</sub> (synonyms: dihydrogen hexafluorozirconate, hydrogen zirconium fluoride) and/or hexafluoro titanic acid, H<sub>2</sub>TiF<sub>6</sub> (synonyms: dihydrogen hexafluorotitanate, hydrogen titanium fluoride) (Table I). To adjust the pH, different acids can be added, usually phosphoric,<sup>29–32</sup> but also boric<sup>33</sup> and nitric acid.<sup>34–37</sup> NaOH or HCl may also be added. In some cases NaF, KF or HF are added to intensify activation,<sup>33,37–39</sup> as fluoride ions attack the surface more strongly than hexafluoro ions.<sup>40</sup> Instead of dihydrogen hexafluoro compounds,<sup>31,34,38,41–73</sup> dipotassium hexafluoro compounds have also been used.<sup>30,32,36,37,40,74–76</sup>

The Ti and/or Zr cations are usually supplied as hexafluoro compounds<sup>30–32,34,36–38,40–59,61–66,68–78</sup> but also as TiCl<sub>4</sub> together with

H<sub>2</sub>SiF<sub>6</sub>,<sup>35</sup> TiCl<sub>3</sub> and H<sub>2</sub>SiF<sub>6</sub>,<sup>79</sup> Zr(NO<sub>3</sub>)<sub>4</sub> and NaF,<sup>33</sup> ZrOCl<sub>2</sub>,<sup>80</sup> Ti(OCH<sub>2</sub>CH<sub>2</sub>CH<sub>2</sub>CH<sub>3</sub>)<sub>4</sub> n-butyl titanate,<sup>76</sup> ZrO(ON<sub>3</sub>)<sub>3</sub>,<sup>81</sup> TiCl<sub>4</sub>,<sup>66,82</sup> and ammonium Zr carbonate C<sub>2</sub>H<sub>10</sub>N<sub>2</sub>O<sub>8</sub>Zr.<sup>63</sup>

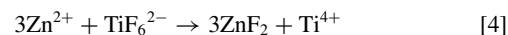
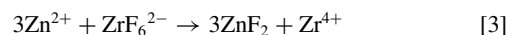
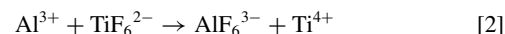
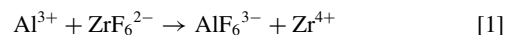
Conversion baths may contain organic additives to increase the adhesion of organic coatings applied on top of the conversion coating, surfactants or inorganic additives such as copper, manganese, phosphate, etc., aiming to increase the kinetics of coating formation, affect the coating structure, or add a functional ability such as self-healing. The effects of additives will be discussed below.

A list of commercial coatings with their trade names and manufacturers, composition and investigated substrates is given in Table II. The coatings are listed chronologically and by the manufacturer. The exact compositions of commercial coating baths are proprietary; the compositions stated herein were taken from the cited references. Some coatings may be the same or similar but the trade name changed with years. According to the compositions given, commercial fluoro conversion coatings are only rarely Ti-based, more often Zr-based, and most often Zr/Ti-based. Some commercial coatings contain trivalent chromium. The majority of commercial coatings were tested on Al alloy substrates.<sup>45,83–95</sup> Fewer studies can be found for these coatings on steels,<sup>6,63,85,96–99</sup> hot-dip galvanized (HDG) steel<sup>43,87</sup> and Mg-based alloys.<sup>100,101</sup>

### Deposition Mechanism

Conversion coatings can be formed by simple immersion in a process bath. The coating formation process for Zr or Ti coatings involves activation of the surface in the acidic fluoride-containing bath and subsequent deposition of the coating. The deposition mechanism has been studied using open circuit potential (OCP) vs. time curves,<sup>6,58,85,87,92,102</sup> mass change,<sup>6</sup> Scanning Kelvin Probe (SKP) maps,<sup>34,55,103</sup> compositional analysis by Fourier transform infrared reflection absorption spectroscopy (FT-IRRAS),<sup>34</sup> Rutherford backscattered spectroscopy (RBS),<sup>49</sup> glow discharge optical emission spectroscopy (GDOES),<sup>49,104</sup> and time-of-flight secondary ion mass spectroscopy (ToF-SIMS), morphological analysis<sup>51,71,88,93–96,103,105</sup> and local pH measurements.<sup>92,106</sup>

Aluminum parts are usually pretreated by alkaline etching and acid de-oxidizing. At that point, the surface of the substrate is covered by a naturally-formed oxide that forms immediately upon exposure to air. Depending on the nature of the substrate, cathodic behavior (indicated by high positive Volta potential) is present at certain phases of the substrate such as intermetallic particles (IMPs). Upon immersion in the fluoride-containing conversion bath of low pH (usually between 2.8 and 4), the aggressive metal hexafluoride ions dissolve the native oxide layer on aluminum and zinc according to:

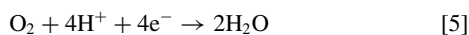


Therefore, the chemical dissolution of the oxide layer by the free hexafluoride ions in the bath represents the first stage of formation of a conversion layer. Different points in the OCP vs. time curves (activation, conversion, precipitation) have been correlated to growth of the layer and its morphology (Fig. 1).<sup>102</sup> In the OCP vs. time curves, the oxide dissolution is reflected as an initial decay in the potential within the first 30–50 s. This process corresponds to surface activation and initiation of the film deposition.<sup>102</sup> The difference between the initial potential and the minimum potential varies for different substrates and is the greatest for Al-based and smallest for steel substrates.<sup>85</sup>

**Table II. Basic composition of commercial Ti-, Ti/Zr- and Zr-based coatings on different substrates.**

Trade name (Manufacturer)	Composition (as given in the paper)	Substrate	Reference
Alodine NR 6217/18 (Gerhard Collardin GmbH)	H <sub>2</sub> ZrF <sub>6</sub> Polyacrylic acid	AlMg0.5	83
Alodine 2840 (Henkel Surface Technologies)	H <sub>2</sub> ZrF <sub>6</sub> + H <sub>2</sub> TiF <sub>6</sub> Polyacrylic acid	AA6060	105
Alodine 1453R (Henkel)	Oxyfluoro Ti, Zr, Si Organic polymer	AA5182	45
Alodine 5700 (Henkel)	Zr oxide and Ti fluoride	AA2024	84
TecTalis (Henkel Corp)	H <sub>2</sub> ZrF <sub>6</sub> + Cu	CRS	6
TecTalis 1800 (Henkel Corp)	H <sub>2</sub> ZrF <sub>6</sub> + Cu	AA6061 carbon steel	93,125
Henkel AG & Co. KGaA	H <sub>2</sub> ZrF <sub>6</sub> + Cu	AA6014, CRS, HDG, AA6014 AA6014, AA1050, AA6016, CRS, HDG	85,86,88,87,108
Bonderite NT-1 (Henkel)	H <sub>2</sub> ZrF <sub>6</sub> , nanoceramic metal oxide particles, pH adjuster	CRS mild steel	96,97,98
Alodine 5200 (Henkel)	Ti-based organometallic zirconate	AM60B, AA2024	100,92
Bonderite MNT 5200 (Henkel)	H <sub>2</sub> ZrF <sub>6</sub> + H <sub>2</sub> TiF <sub>6</sub> (1:3)	AA2024	106
Alodine 4830 (Henkel)	H <sub>2</sub> ZrF <sub>6</sub> + H <sub>2</sub> TiF <sub>6</sub>	AA6061	89
Bonderite 5200 (Henkel)	Cr-free hexafluoro-titanate/zirconate type + organic polymer beads	AZ31, ZE10A	127
Granodine 1445 T (Henkel)	dihydrogen hexafluorotitanate phosphoric acid organic compounds	HD Al-Si steel	102
Bonder D6800 (Chemetall)	H <sub>2</sub> ZrF <sub>6</sub>	HDG and Galfan coated steel	43
Gardobond X4591 (Chemetall)	H <sub>2</sub> TiF <sub>6</sub> + H <sub>2</sub> ZrF <sub>6</sub>	Al	90
Gardobond X4707 (Chemetall)	H <sub>2</sub> TiF <sub>6</sub> + H <sub>2</sub> ZrF <sub>6</sub>	AA6060	94,95
Gardobond X4705 (Chemetall)	(Zr(OBu <sup>n</sup> ) <sub>4</sub> ) + acetic acid + ZrO(NO <sub>3</sub> )	AA1050	91
TCP (Navair)	Zr fluoride and Cr(III) sulfate	AA2024	84
NCP (Navair)	H <sub>2</sub> ZrF <sub>6</sub> + ZnSO <sub>4</sub>	AA2024, AA6061, AA7075	112
Surtec 650 (Surtec International)	H <sub>2</sub> ZrF <sub>6</sub> + Cr(III)	AZ31, ZE10A	101
MAVOMcoat 1742 CC (MAVOM Chemie BV)	H <sub>2</sub> ZrF <sub>6</sub>	CRS	99
PreCoat A32	H <sub>2</sub> ZrF <sub>6</sub> + Cr(III)	AA2024-T3, AA2024-T81	128

The reactions of oxygen reduction and hydrogen evolution take place at cathodic sites:



These cathodic reactions cause local alkalization. The interfacial pH change measured using a tungsten oxide pH microelectrode at

the surface of AA2024 during Ti-based conversion coating treatment increased from ca. 2.5 to 8.5 (Fig. 2).<sup>92,106</sup> This increase in pH drives the hydrolysis of the fluorometalates to form precipitated hydrated metal oxide layers. Therefore, the deposition of oxides is a pH-driven process. The deposition reactions can be generally presented as:<sup>92,106</sup>

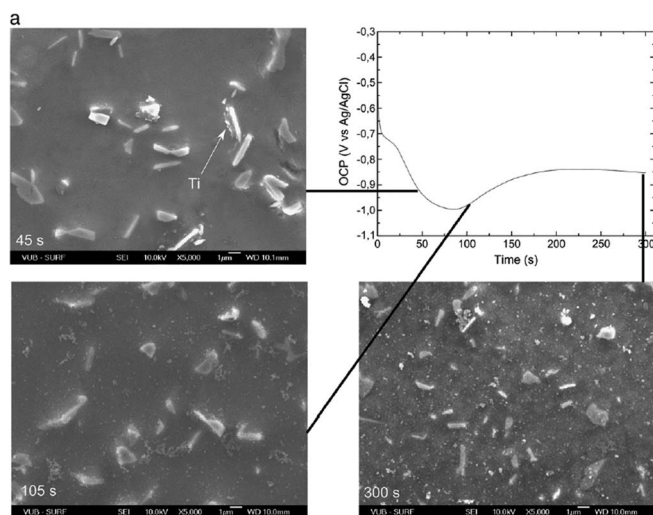
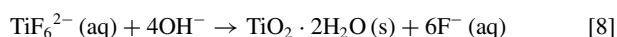
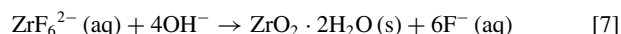


**Figure 1.** Secondary electron images of the deposition of Ti-based coating on hot dip Al-Si coated steel taken at different time of immersion in conversion bath and OCP vs. time curve. Reprinted from the publication by I. Schoukens, I. Vandendael, J. De Strycker, A.A. Saleh, H. Terryn, and I. De Graeve, *Surf. Coat. Technol.*, **234**, 628–636 (2013) with permission from Elsevier.<sup>102</sup>

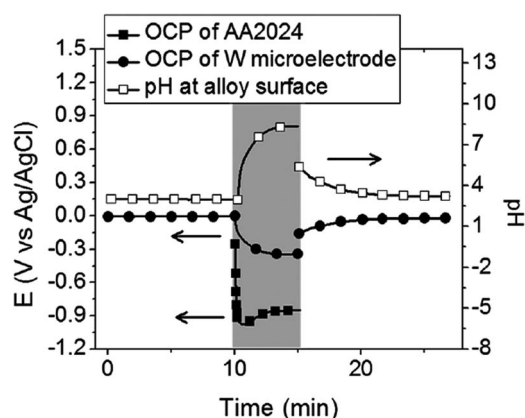
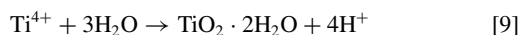


**Figure 2.** A typical trace at the AA2024 surface (empty squares, right y-axis) before, during and after formation of the Alodine 5200 coating (Ti-based). The OCP of the W/Wo<sub>3</sub> microelectrode and the AA2024 sample (solid circles and squares, respectively, left y-axis) are also shown. Formation of the coating occurred between 10 and 16 min as shown by the gray shaded background. Reprinted from the publication by L. Li, A.L. Desouza, and G.M. Swain, *Analyst*, **138**, 4398–4402 (2013) with permission from Royal Society of Chemistry.<sup>92</sup>



and



It should be noted, however, that the precipitated product may also contain suboxides, oxyhydroxides and other compounds like fluorides, as will be discussed in Composition section. Zirconium- and titanium-based conversion coatings follow a similar deposition route. Precipitation and lateral growth of the conversion layer corresponds to a minimum in the OCP vs. time curve (Fig. 1). In this region, the precipitation rate of conversion coating starts to prevail over metal dissolution. The subsequent plateau region of the OCP (reached after ~200 s) denotes that a steady state deposition process is reached followed by extensive surface coverage by the conversion coating. Further deposition is expected to lead to an increase in layer thickness without a change in potential.

Due to differences in Volta potential compared to matrix, IMPs or cathodic phases are the sites where cathodic reaction takes place.<sup>72,87,99,103</sup> The consequent pH increase then creates the conditions for the deposition of oxides, which starts preferentially at the location of cathodic sites about 60 s after immersion (Fig. 3).<sup>107</sup> The initial difference in Volta potential of several hundreds mV at the beginning of conversion decreases to only 5 mV once the coating entirely covers the surface.<sup>6,107</sup> The conversion process is self-limiting, i.e. when the driving force (potential) decreases, the process ceases.

### Conversion Bath Parameters

**pH and time of immersion.**—The bath pH strongly affects the uniformity of the coating formed during conversion and the resulting coating properties. The pH of 4.0 was used in the vast majority of reports.<sup>6,36,37,42,51,52,55–57,61,62,65,68,75,85–88,94,98,108,109</sup> although conversion was carried out at pH between 1.5 and 6.<sup>30,32,46,48,49,53,64,66,68–70,77,78,82,90,95,99,106,107,110</sup> More extensive and thicker coating formation at pH 4.0 than at 2.9 was noticed for Gardabond X4707 coating on AA6060.<sup>94</sup> The coating formed at pH 4 showed lower cathodic current density compared to that formed at 2.9. The concentration of Zr and Ti in the coating increased with the pH of conversion bath.<sup>38</sup> Increasing the pH from 2.5 to 4.5 during the formation of Zr-based coatings on AA1050 resulted in the decrease in OCP values in regions of surface activation and Zr conversion.<sup>64</sup>

The effect of immersion time was investigated in numerous studies to obtain the optimal coating parameters in terms of morphology, composition, thickness and corrosion resistance.<sup>6,32,34,55,37,50,52,55,61,63,69,73,77–79,88,90,93,94,96,102,107,110</sup> The immersion time of metal substrates in conversion baths ranged from less than 3 minutes,<sup>31,38,42,46,48,51,57,59,65,67,70–72,85,86,95,97,101,106</sup> and between 3 and 6 minutes.<sup>30,47,53,64,78,87,110–112</sup> Longer immersion times, from 10 up to 25 min, were also investigated.<sup>36,49,50,75,80,81</sup> It seems, however, that immersion times were greater than 10 min in baths not containing F<sup>−</sup>, e.g. (ZrOCl<sub>2</sub>)<sup>75</sup> and ZrO(NO<sub>3</sub>)<sub>3</sub>.<sup>81</sup>

In general, longer immersion time produced more uniform and thicker conversion layers. To form Zr/Ti layers on Al of measurable thickness, determined by ellipsometry, an immersion time of at least 90 s was required.<sup>90</sup> After 600 s, the thickness of 70 nm was reached.<sup>90</sup> Andreatta et al. studied the effect of immersion time on morphology, composition and Volta potential of Ti/Zr-based coatings on AA6016.<sup>107</sup> After 120 s, the coatings formed mainly on IMPs and the Volta potential decreased to 280 mV (compared to > 400 mV on bare etched substrates) (Fig. 3). When the immersion time was increased up to 300 s, the coating covered the entire surface and was accompanied by a decrease of Volta potential difference to only 5 mV. Progressive coverage of the substrate surface with increasing immersion time was generally noticed.<sup>69,73</sup> SEM images recorded on AA6014 substrate immersed in H<sub>2</sub>ZrF<sub>6</sub> bath containing Cu for various immersion times up to 120 s are presented in Fig. 4.<sup>88</sup> In some studies it was noticed that, although the coatings were thicker at longer im-

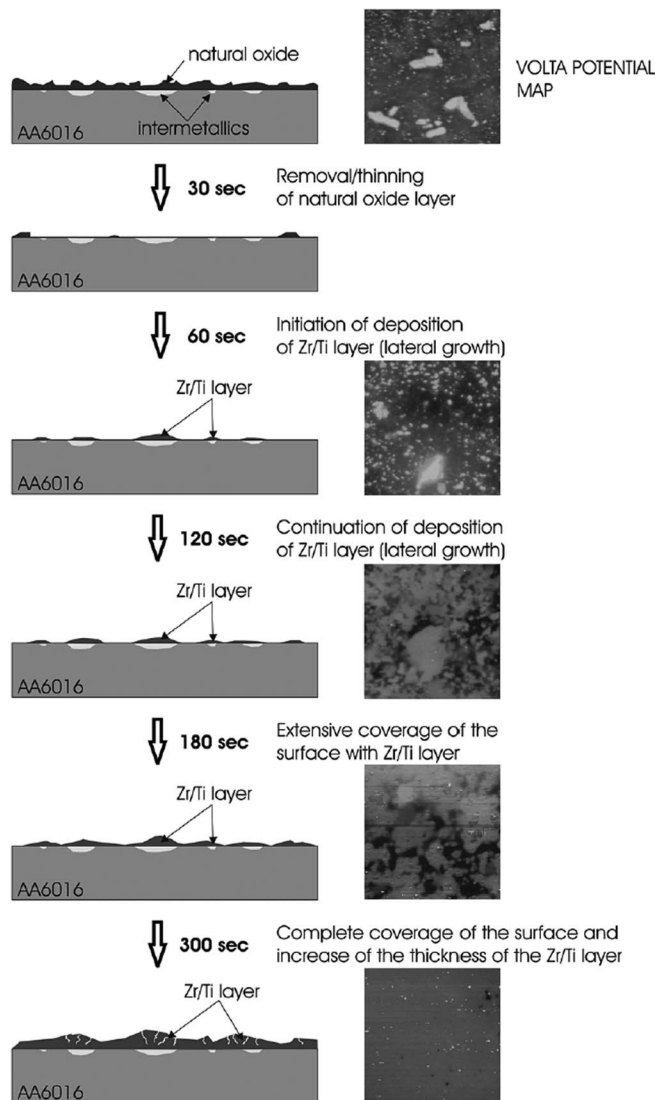


**Figure 3.** Mechanism of deposition of Zr/Ti layer on AA6016: schematic presentation of course of formation of conversion coating (left panel), and Volta potential map as a function of time of immersion in conversion bath (right panel). Reprinted from the publication by F. Andreatta, A. Turco, I. de Graeve, H. Terryn, J.H.W. de Wit, and L. Fedrizzi, *Surf. Coat. Technol.*, **201**, 7668–7685 (2007) with permission from Elsevier.<sup>107</sup>

mersion time, cracks appeared, probably as a result of internal stress in thick films as the layer dried.<sup>57,52,60,79,96</sup>

Khun et al. measured surface roughness as a function of immersion time during formation of TecTalis coating on AA6061<sup>93</sup> and low carbon steel.<sup>63</sup> The roughness increased with immersion time up to 60 s as a result of the nucleation, clustering and growth of zirconia nodules.<sup>93</sup> For longer immersion times, the surface roughness decreased through the improved uniformity of the oxide layer.<sup>93</sup> The increase in surface roughness of Zr/Ti-based coatings with immersion time was beneficial to improve adhesion strength of the organic coatings by physical interactions.<sup>69</sup>

**Temperature.**—In the majority of studies the conversion process was carried out at room temperature (20–25°C), which minimizes energy costs for industrial processes.<sup>33,34,36,37,47,51,52,55,59,61,62,64–66,69,70,72,78,82,84,87,90,92,94,95,98,99,101,102,104,106–108,110,112–114</sup> Elevated temperatures were also studied, i.e. between 30 and 55°C.<sup>6,30,42,46,48,49,53,57,63,67,75,77,79,81,93,111</sup> The conversion bath temperature was varied in several studies to determine the optimal value in

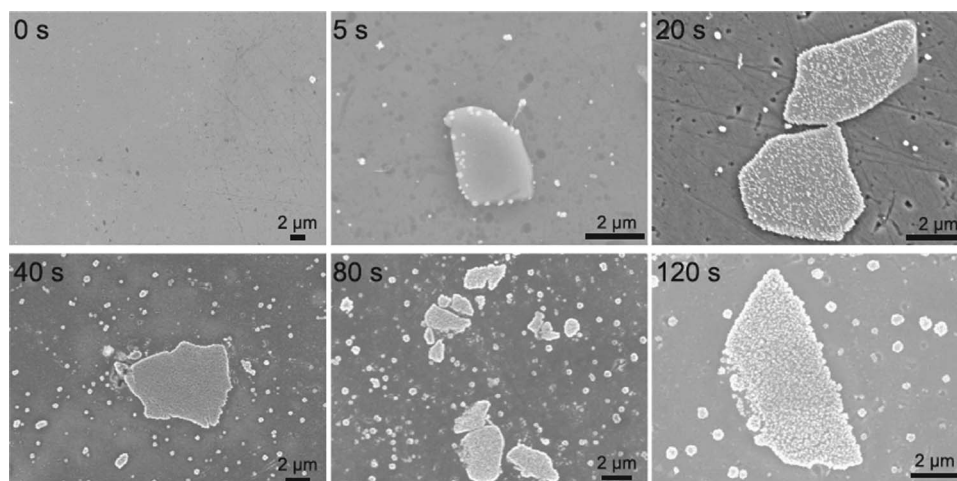


**Figure 4.** SEM images of AA6014 substrates pre-treated after different immersion time using Zr-based coating. Reprinted from the publication by A. Sarfraz, R. Posner, M.M. Lange, K. Lill, and A. Erbe, *J. Electrochem. Soc.*, **161**, C509–C516 (2014) with permission from Electrochemical Society.<sup>88</sup>

terms of morphology, composition and corrosion resistance.<sup>32,35,43,58,96</sup> The optimal conditions were different for different coatings. On HDG and Galvan coated steel, 40°C was found to be optimal in terms of the Zr concentration in the coating.<sup>43</sup> For other types of Zr-based coatings deposited on cold rolled steel (CRS)<sup>96,97</sup> and AA1050,<sup>58</sup> the optimal temperature was 20°C, as it exhibited lower corrosion current density,  $i_{\text{corr}}$ , compared to coatings formed at 30°C and 40°C. Ti-based coatings on electrogalvanized galvanized steel samples treated at 50°C exhibited the longest time to formation of the first white rust.<sup>35</sup> Similarly, Ti-based coatings containing Mn(III) phosphate and deposited on Zn coated steel exhibited lower  $i_{\text{corr}}$  when prepared at 60°C than at lower temperatures.<sup>32</sup>

**Bath agitation.**—In only a few studies<sup>35,52,87,95,99,107</sup> was the conversion bath agitated by stirring during deposition; most baths were stagnant. Recent studies have shown, however, that convection significantly affects the properties of the coating.<sup>99,108</sup> For Zr-based coatings on AA6014 and CRS, thickness increased several times as a result of stirring at 400 rpm.<sup>108</sup> Convection affects the coating conversion kinetics by supplying higher concentrations of fluorides at the substrate surface as a result of accelerated mass transport. This reduces the time required for oxide dissolution and increases the available time zirconium can deposit on the activated matrix.<sup>108</sup> Moreover, the content of copper in the coating, coming from  $\text{Cu}^{2+}$  added to conversion bath to increase the number of cathodic sites at the surfaces, is enriched on the surface with stirring.

Summarizing, conversion bath parameters (composition, pH, temperature and bath agitation) strongly affect the coating properties such as coating composition, morphology, thickness and corrosion resistance, as will be discussed below. Optimal conditions are typically pH 4, time of immersion between 2 and 5 min and temperature between room temperature and 50°C. The conversion baths have usually been left stagnant during deposition.

### Conversion Bath Additives

**Organic additives.**—The aims of organic polymer additives are to improve adhesion to the underlying substrate, to improve homogeneity of the coating and to establish a base for subsequent organic coatings. Early studies mainly incorporated poly(acrylic acid) (PAA)<sup>19,41,83</sup> and pyrrolidine-based polymer.<sup>34</sup> The choice of polymer was reported to be critical to ensure good coating performance.<sup>42</sup> Polymers had more impact on the polyester paint adhesion than the cation (Ti or Zr) of the coating.<sup>42</sup> A given polymer, however, is more effective in a Zr-based coating than in a Ti-based one due to the ability of Zr to act as a cross-linking agent. When treated in baths without polymers,

the coatings were nonhomogeneous and exhibited worse corrosion resistance in 3% NaCl.<sup>42</sup> The presence of PAA in the bath resulted in the 2D formation of polymer film preferentially on Zr-Ti oxide. Its formation was ascribed to physical and/or chemical interactions.<sup>105</sup> Defects at the surface may act as nucleation sites for polymer film formation. After nucleation, which may be favored at hydroxide sites, rapid 2D growth of polymer takes place, extending farther than the precipitated Zr-Ti oxide.

Coatings from baths with various blends of  $\text{H}_2\text{ZrF}_6$ , PAA and polyacrylic amide (PAM) were prepared to investigate their effect on the performance when subsequently coated with epoxy.<sup>47</sup> The addition of both PAA and PAM to Zr-based coatings improved the corrosion resistance compared to the individual polymers alone. Additives like polyvinyl phenol phosphate,<sup>54</sup> silane<sup>104</sup> and polypyrrole<sup>29</sup> were also added to conversion baths.

Instead of polymers, various chelating agents may be used to enrich the coating composition. Amino trimethylene phosphonic acid (ATMP) is a powerful chelating agent and was used to improve lacquer adhesion and corrosion resistance of Zr- and Ti-based coatings on AA6061.<sup>46</sup> Such hybrid coatings were denser; phosphonate was formed along with Ti-Zr oxides. Phytic acid is a harmless, large organic chelating molecule that forms stable metal-phytic complexes.<sup>67</sup> Coatings containing phytic acid exhibited reduced wettability and higher adhesion to an epoxy topcoat than Ti conversion coatings alone. Reduced adhesion loss was ascribed to the improved bonding between epoxy coating and phytic-containing coating, i.e. a chelate reaction between  $\text{Fe}^{2+}$  or  $\text{Fe}^{3+}$  and phytic acid.

Tannic acid (TA),  $\text{C}_{76}\text{H}_{52}\text{O}_{46}$ , a type of polyphenol, has been used to improve adhesion on steel and zinc since the 19<sup>th</sup> century. Metal tannates and tannate complexes formed with metal and metal oxides improved adhesion to the substrate although the level of protection was not substantial.<sup>115–117</sup> TA has been recently considered as a corrosion inhibitor for various metals and alloys.<sup>118</sup> Smit et al. added TA (40 g/L) to a Ti-based conversion bath instead of PAA to form coatings on AA3003.<sup>44</sup> Corrosion protection was found only for immersion times up to 10 h; longer immersion led to deterioration due to dissolution of the organic component. TA (2–3 g/L) was added to a mixed Ti/Zr fluoro conversion coating on AA6063<sup>50,61</sup> and galvanized steel.<sup>78</sup> A double layer structure was postulated with metal–organic complexes located primarily in the outer layer of the conversion coating, and an inner layer made mainly of  $\text{Na}_3\text{AlF}_6$ ,  $\text{TiO}_2$ ,  $\text{Al}_2\text{O}_3$ , etc.<sup>60</sup>

**Combined organic and inorganic additives.**—The combined action of organic and inorganic additives was studied for Ti-based coatings on HDG steel.<sup>31,72</sup> The organic component was mainly poly-(4-vinylphenol) but linked to the amino group of quaternary ammonium

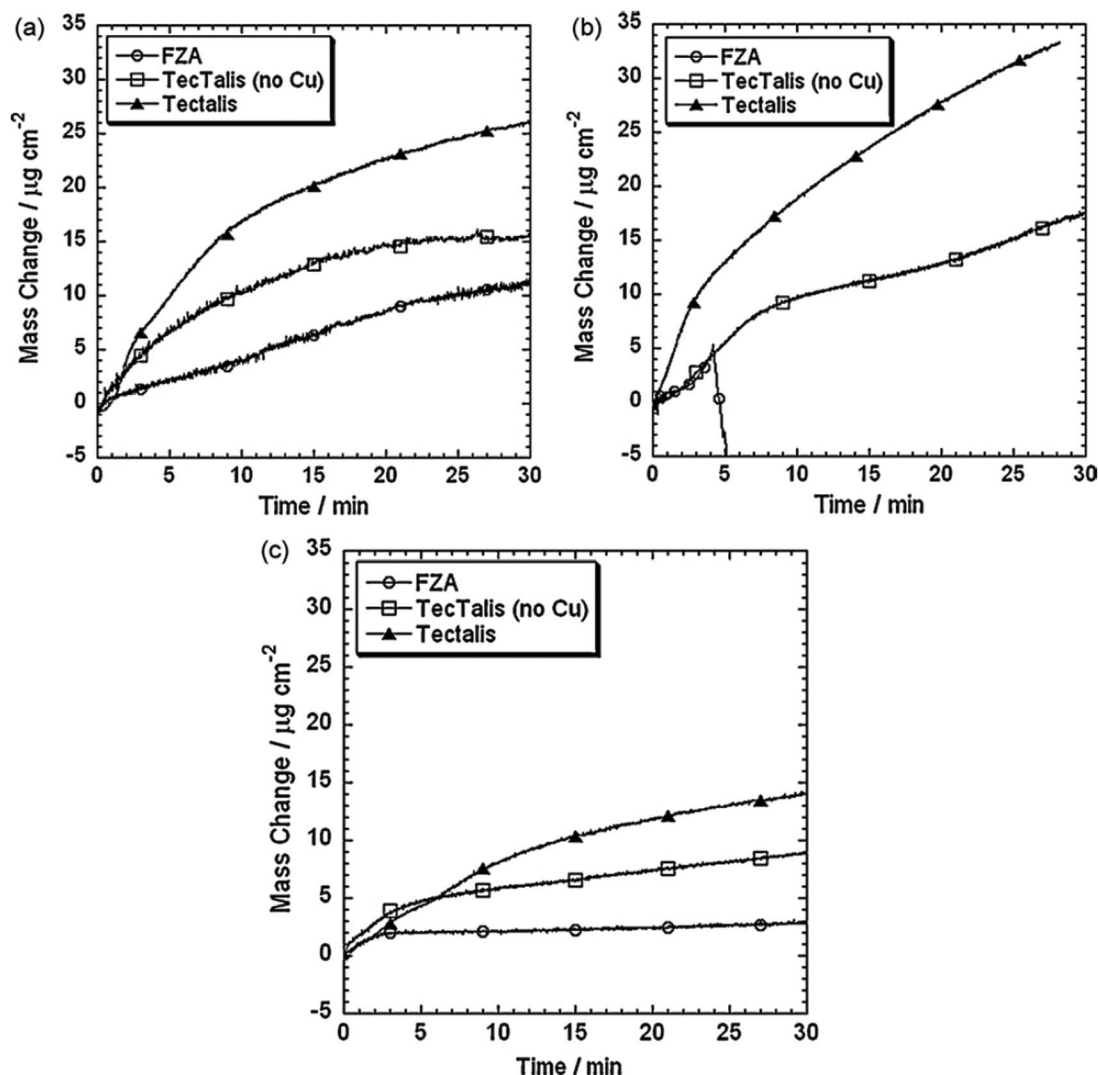


**Figure 5.** Quartz microbalance mass gain for (a) Fe, (b) Al and (c) Zn in hexafluorozirconic acid (FZA), Tectalis without Cu and TecTalis. Reprinted from the publication by S. Adhikari, K.A. Unocic, Y. Zhai, G.S. Frankel, J. Zimmerman, and W. Frisstad, *Electrochim. Acta*, **56**, 1912–1924 (2011) with permission from Elsevier.<sup>6</sup>

and N-methyl glucamine;<sup>31</sup> the inorganic component was manganese phosphate,  $\text{Mn}_3(\text{PO}_4)_2$ . The polymeric layer acted as a surfactant resulting in the formation of organic-inorganic adlayer, which presumably started to nucleate at titanium oxide islands (as shown by Nordlien et al.).<sup>105</sup> The role of the organic phase was to coordinate the layer conversion and thus assist in achieving a more homogeneous layer.<sup>72</sup> The homogeneity, morphology and corrosion resistance of the coating was satisfactory only when the inorganic and organic components were both present; the addition of  $\text{Mn}_3(\text{PO}_4)_2$  limits the bath acidity at 2.9 and thus stabilizes the layers, as will be discussed below. Quaternary amine groups and N-methyl glucamine rich hydroxide groups are expected to react with metallic species on the HDG steel surface to form organic/inorganic complexes.<sup>31</sup> Consequently, polymer adsorption on the substrate was improved.

**Inorganic additives.—Copper.**—Cupric ions can be added to the conversion bath with the aim of forming Cu deposits on the metal surface, which serve as additional cathodic sites for the reduction reaction during conversion and thus accelerate the subsequent increase in pH and promote the deposition of Ti- and Zr-hydroxides. In several studies, the commercial hexafluorozirconic acid-based baths containing some amount of copper were investigated.<sup>6,62,85–88,108</sup> When properly activated, even if the alloy itself does not contain copper (e.g. in

AA1050), Cu-rich particles will deposit on the surface and promote the formation of Zr-based coating.<sup>87</sup> The TecTalis coating containing Cu deposited on CRS was thicker compared to that without Cu (30 nm and 20 nm, respectively).<sup>6</sup> Copper was enriched, even up to 50–60 wt% at some locations. The Cu deposits were randomly distributed and not restricted to any specific locations within the coating. The content of Cu in the coating significantly increased with agitation of the conversion bath, i.e. by a factor of 3 on CRS and HDG steel substrates, and by a factor of 0.5 on AA6014.<sup>108</sup>

The content of Cu in the coating differed depending on the substrate. Areas with different concentrations of Cu were observed on AA6014, with islands of copper (0.2 to 2  $\mu\text{m}$ ) greater in size than those observed for CR and HDG steels.<sup>85,86</sup> Cu particles were visible after only 5 s of deposition and then grew in size and density with increasing conversion time.<sup>88</sup> Copper was present both in the metallic form and as CuO. The presence of CuO on the surface and inside the coating suggests that Cu deposited in the metallic form, but subsequently oxidized, either in the conversion bath or upon contact with air.<sup>88</sup> Nucleation is thus instantaneous, preferentially at boundaries of intermetallics and is followed by growth of Cu-rich particles in the lateral direction.

The mass gains measured by quartz microbalance on the pure metals Fe, Al and Zn in  $\text{H}_2\text{ZrF}_6$  conversion baths with and without Cu



are presented in Fig. 5.<sup>6</sup> The deposition rate was always the highest for Al followed by Fe and Zn, and was highest when Cu was present in the conversion bath. At shorter formation times (60 s), the TecTalis coating contained Cu, Cu<sub>2</sub>O and CuO.<sup>63</sup> At longer times (180 s) the content of CuO decreased, indicating that prolonged treatment promotes the formation of Cu<sub>2</sub>O in the ZrO<sub>2</sub> layer. The behavior on alloys can be different as discussed below.

The literature contains some inconsistencies regarding the influence of Cu ions in the coating bath on the corrosion performance of the conversion coating. In terms of corrosion performance, Adhikari et al.<sup>6</sup> reported that TecTalis coatings deposited on steel both with and without Cu showed high impedance values for up to 120 days in 0.5 M NaCl when coated with electrodeposited paint. However, the coating containing Cu provided a significantly improved resistance to delamination.<sup>6</sup> On the other hand, the addition of Cu ions added as Cu(NO<sub>3</sub>)<sub>2</sub> to hexafluorotitanium baths containing silane agent worsened the corrosion protection of AA6014-T4.<sup>104</sup> Although the layer was thicker, it may have been less homogeneous and thus less protective. Lostak et al. studied the effect of Cu<sup>2+</sup> and Fe<sup>3+</sup> added as nitrates to Zr-based coatings on HDG steel.<sup>52</sup> The addition of Cu<sup>2+</sup> led to a thicker, but more inhomogeneous, Zr oxide layer compared to the addition of Fe<sup>3+</sup>, especially at shorter deposition times (60 s). The addition of Cu<sup>2+</sup> and Fe<sup>3+</sup> shifted the OCP more positive because of their oxidizing power and the generation of micro-cathodes.

**Zinc and manganese.**—The non-chromium process (NCP) coating developed by NAVAIR (Naval Air Systems Command) is a chromium-free zirconium- and zinc-based coating used as a primer for aluminum alloys in a ready-to-use form.<sup>112</sup> Both Zr- and Zn-deposits are formed around Cu-rich IMPs and Zn is present throughout the coating at about 10 at.% but is elevated at the outer interface. In aggressive corrosion testing, NCP coating performed worse than a commercial trivalent chromium process (TCP) chromium(III)-based coating, which was ascribed to the higher solubility of Zr(OH)<sub>4</sub> and Zn(OH)<sub>2</sub> and reduced adhesion strength compared to Cr(OH)<sub>3</sub> in the TCP coating.<sup>112</sup>

Reducible hypervalent transition metals (Mo, Mn, V, Te) were considered as possible chromate replacements, because they, like Cr, form oxoanions in aqueous solution. Anions of Mo and Mn are very soluble and undergo reduction to insoluble products, which could provide extra protection during formation of conversion coatings.<sup>74</sup> Manganese was added in the form of phosphate,<sup>31,72</sup> nitrate<sup>32</sup> and sulfate.<sup>57</sup> The homogeneity, morphology and corrosion resistance of the Ti-based conversion coating containing manganese(II) phosphate was satisfactory only when the inorganic component was present along with an organic one.<sup>31,72</sup> The addition of Mn<sub>3</sub>(PO<sub>4</sub>)<sub>2</sub> limits the bath acidity at pH 2.9; in its absence the pH was 2.4. The pH of 2.9 was essential for precipitation leading to homogeneous formation of the conversion oxide layer, as precipitation of the coating was destabilized below pH 2.9. The conversion layer consisted of precipitated Zn, Ti and Mn as oxide/hydroxides and phosphates. The latter promoted polymer adsorption on the HDG steel substrate.<sup>31</sup>

The effect of manganese sulfate concentration in Zr-based conversion baths on the coating formed on carbon steel was studied.<sup>57</sup> Only the lowest Mn<sup>2+</sup> concentration improved corrosion characteristics compared to the coating from an unmodified Zr-based bath. It was suggested that Mn<sup>2+</sup> reduced cracks in the coating and resulted in more uniform surface coverage when present at low concentration but destabilized the layer formation at higher concentration. Manganese ions added to a Ti/Zr conversion bath may act like a catalyst for the conversion coating formation.<sup>61</sup> First, MnOOH precipitates on the surface of AA6063 substrate and provides nuclei for Na<sub>3</sub>AlF<sub>6</sub> crystals that form around them. With increasing conversion time, Na<sub>3</sub>AlF<sub>6</sub> crystals grow continuously and progressively the conversion coating covers the entire surface.

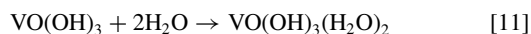
**Nickel, molybdenum and phosphorus.**—The effect of Ni and Mo added as sulfates in Ti-based composite conversion coating baths was studied on CRS.<sup>82</sup> Coatings modified by Ni exhibited lower corrosion current density and higher polarization resistance than coatings modi-

fied by Mo or unmodified coatings. A Ni oxide or hydroxide layer was formed as an outer layer of the TiO<sub>2</sub> coating and presumably acted as a physical barrier. On the other hand, a thick cracked layer containing Mo in both Mo<sup>6+</sup> and Mo<sup>4+</sup> oxidation states precipitated at the CRS surface. The formation of cracks was ascribed to release of hydrogen from dehydration of the molybdate conversion coating.<sup>82</sup>

In another paper, two approaches were tested for Zr-based coatings on galvanized steel:<sup>68</sup> Zr and Ni mixed in the conversion bath (Zr+Ni), or prepared as two separate layers (Zr/Ni). Mixed Zr+Ni coatings performed worse than the unmodified Zr coating. Due to their similar size, Zr<sup>4+</sup> and Ni<sup>2+</sup> ions compete for deposition at the cathodic sites and cause inhomogeneities in the layer, as was noted also for Mn<sup>2+</sup>.<sup>57</sup>

Some Zr/Ti conversion coatings contain phosphates.<sup>29–32,36,37,54,67,72,102,104,111</sup> Along with the deposition of oxide, hydroxide and fluoride compounds, phosphates can be also formed during conversion process.<sup>30,32,37,67,72,102</sup> Andreatta et al. reported that the addition of phosphates strongly improved the barrier properties of the coatings due to deposition of phosphate species on the substrate.<sup>104</sup>

**Vanadium, cerium and chromium.**—Vanadium has been added to conversion baths in both the metavanadate form, as NH<sub>4</sub>VO<sub>3</sub><sup>36,37</sup> and as NaVO<sub>3</sub>.<sup>59,69,70</sup> The V-modified Ti/Zr coating exhibited superior electrochemical characteristics and improved the adhesive strength of an organic epoxy coating.<sup>36,69</sup> The self-repairing ability of VO<sub>3</sub><sup>–</sup>-containing Zr-based conversion coatings deposited on AA6063 was studied by Zhong et al.<sup>53</sup> X-ray photoelectron spectra (XPS) identified the formation of V<sup>4+</sup> and V<sup>5+</sup> compounds linked to ZrO<sub>2</sub>. Due to the oxidative action of H<sub>2</sub>O<sub>2</sub>, V<sup>5+</sup> ions can exist and convert into hydrate, which can be transferred to the part of the surface where localized attack occurs:



In this sense, V<sup>5+</sup> ions act similar to Cr<sup>6+</sup> ions. The repair effect was lost after 5 d immersion in NaCl solution.

Vanadium pentoxide, V<sub>2</sub>O<sub>5</sub>, was added to Zr-based hybrid conversion baths that also included inorganic ammonium zirconium carbonate, organic cyclic-amine-containing polymer (CAP), and ascorbic acid.<sup>119</sup> Because ascorbic acid was present, V<sup>5+</sup> could be reduced to V<sup>4+</sup>.<sup>119</sup> The coating containing both CAP and V showed the best corrosion performance in the salt spray chamber. It was suggested that co-incorporation of CAP and V gave rise to more effective coating inhibition via controlled release of V, and an ability to repair scribes through the coating.

Another possibility to achieve the self-repair functionality of Zr-based conversion coating is to add cerium ions. Cerium(III) nitrate was added to conversion bath containing zirconyl nitrate ZrO(NO<sub>3</sub>)<sub>2</sub>, H<sub>2</sub>O<sub>2</sub> and Ce(NO<sub>3</sub>)<sub>3</sub> and deposited on AA2024.<sup>81</sup> It was suggested that deposition of Ce oxide/hydroxide (CeO<sub>2</sub> and Ce(OH)<sub>4</sub> and Ce(OH)<sub>3</sub>) occurs simultaneously with deposition of ZrO<sub>2</sub>. This was reflected in smaller *i*<sub>corr</sub> values exhibited by the Ce-containing coating even after 168 h immersion in 0.6 M NaCl. A simulated scratch cell test showed self-healing ability as the charge transfer resistance gradually increased for up to 336 h followed by repair of defects (Fig. 6). After 168 h in salt spray testing, these coatings were comparable to chromate conversion coatings.

A conversion coating containing Cr(III) was found to exhibit self-repairing property,<sup>120</sup> which other researchers suggested might be due to local production of H<sub>2</sub>O<sub>2</sub> that can then oxidize Cr(III) to Cr(VI) and lead to self-repair.<sup>121,122</sup> Based on that information, Zr- and Cr(III)-containing conversion coatings on AA2024-T3 were prepared to achieve self-repairing.<sup>75</sup> After 3 days exposure to ammonium sulfate and sodium chloride solution in an artificial scratch test cell, only Cr species were present at the surface, proving that these species were responsible for the self-repairing effect.

Summarizing, organic additives are beneficial to reduce cracking of the coating, to increase the coating density and improve adhesion to organic topcoat. Inorganic additives affect the deposition kinetics by



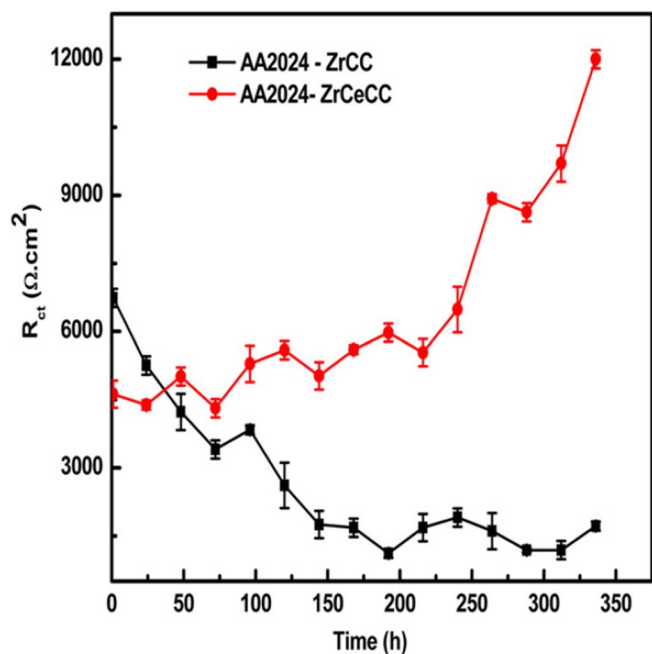


**Figure 6.** Charge transfer resistance value versus immersion time of AA2024 coated with Zr conversion coating, ZrCC, and Zr-coating containing cerium, ZrCeCC, exposed to simulated scratch cell. Reprinted from the publication by G. Yoganandan, K. Pradeep Premkumar, and J.N. Balaraju, *Surf. Coat. Technol.*, 270, 249–258 (2015) with permission from Elsevier.<sup>81</sup>

providing additional cathodic reaction sites (Cu), blocking the active sites by formation of insoluble oxides (Mn, Mo) creating nucleation sites for Al-fluoride (Mn), improving barrier properties (Ni), promoting adhesion (phosphate), and providing a self-healing agent (V, Ce, Cr).

### Effect of Substrate on Coating Formation

The mechanism of conversion coating deposition is dependent on the substrate because the substrate must be activated, i.e. dissolved, to initiate the conversion process. Dissolved metal ions can then precipitate and be incorporated in the conversion coating, at the interfacial region or throughout the coating. In this section, the reactions taking place on different substrates during coating formation are discussed.

**Effect of substrate pre-treatment and surface chemistry on coating formation.**—In general, the coating formation proceeds in 5 stages:<sup>123</sup> “clean-rinse-coat-rinse-dry”. The procedures within individual stages vary from study to study. The “clean” stage consists of pre-treatment of the samples to properly prepare the surface for subsequent formation of the conversion layer. Pre-treatment may include both mechanical and chemical treatment, an intermediate rinsing step, followed by coating formation, rinsing and drying. Usually, all the steps are included in the procedure, but variations are possible. Mechanical pre-treatment in the form of grinding and/or polishing may precede chemical pre-treatment but chemical pre-treatment is often applied without prior mechanical treatment. In some cases, the surface was not mechanically pre-treated but cleaned with ethanol<sup>102</sup> or acetone,<sup>55,65,68,98,99</sup> rinsed and coated.

Chemical pre-treatment may include: alkaline degreasing or etching,<sup>34,36,37,42,43,50,52–54,57,60,61,63,66,67,82,85,88,92,93,96,97,108,114,119,124,125</sup> alkaline degreasing or etching followed by acid desmutting or deoxidation,<sup>6,30,47,58,59,64,74–77,81,84,89,94,95,104–106,112,124</sup> and acid cleaning or activation.<sup>32,35,44,46,69,70,77,79,107,124</sup> Various commercial and non-commercial chemical formulations were used as alkaline and acid agents.

For rinsing, deionized water is usually used, although also tap water<sup>92,94,106,112</sup> was applied to make the procedure simpler for industrial processing. Due to environmental and health concerns related to toxicity and carcinogenicity of chromates, procedures that reduce the worker exposure and discharge into the environment were introduced. These are so called “no-rinse” or “dried-in-place” chrome treatments.<sup>42</sup> For these, the rinsing step is excluded between coating formation and drying so that the use of water and waste burden is minimized. Zr/Ti-based conversion coatings can be prepared in conventional or “dried-in-place” technology<sup>41,44</sup> or “ready-to-coat”.<sup>112</sup>

Surface chemistry resulting from the “clean” step affects the subsequent “coat” step. Better Ti-based conversion coatings were obtained when acid cleaning was used instead of alkaline cleaning as a pre-treatment for AA5005.<sup>77</sup> The coating contained a higher concentration of Ti and formed a more continuous layer. Alkaline cleaning followed by acid pickling was more effective than alkaline cleaning as a pre-treatment for fluorotitanate or fluorozirconate coatings.<sup>124</sup> In contrast, the type of chemical pre-treatment was not crucial for chromate coatings.<sup>124</sup>

De-alloying, which occurs at and around most intermetallic particles in the Al matrix during acid or alkaline cleaning, results in the formation of Cu-rich particles and clusters. The amount of Cu-rich particles was higher after acid pre-treatment.<sup>87</sup> During conversion, the Cu-rich particles grow in size and, at and around these Cu-rich zones, the thickness of the Zr-based coating is at least two times higher than the one obtained without Cu deposits. When the surface was thermally pre-treated, i.e. was covered by an oxide layer and not activated, the presence of Cu in the conversion bath could not stimulate the formation of Zr deposition process. Therefore, surface activation is crucial for subsequent coating deposition.

The hydroxyl fraction on the surface was reported to have an important effect on subsequent coating formation. Samples of varying hydroxyl fractions were prepared by different pre-treatments.<sup>51,62,86,87</sup> For lower  $\text{OH}^-$  fractions, less-developed conversion coatings were formed, whereas coating formation was promoted on samples with higher  $\text{OH}^-$  fractions.<sup>86</sup> This was related to the first stage of coating formation, dissolution of oxide from interaction of free fluoride with hydroxyl group and formation of Al–F complex. For samples with high hydroxyl fraction, this occurred readily, at an earlier stage of coating formation, allowing more time for the deposition stage within the timeframe of the coating formation.

**Aluminum alloys.**—Many reactions may take place when Al alloy is exposed to a conversion bath, leading to the formation of various compounds at the concentration of several at.% including  $\text{Al}_2\text{O}_3$  and  $\text{AlOF}$ ,<sup>41,42</sup>  $\text{AlF}_3$  and  $\text{AlOOH}$ ,<sup>40</sup>  $\text{Al}_2\text{O}_3$  and  $\text{AlF}_3$ ,<sup>46,59,69,89</sup>  $\text{Al}_2\text{O}_3$  and  $\text{Na}_3\text{AlF}_6$ ,<sup>30,50</sup> and  $\text{AlPO}_4$ .<sup>30</sup> An example of a depth profile of Zr-based coating formed on Al-alloy is presented in Fig. 7a.<sup>108</sup>

For Al alloys in the 1xxx, 3xxx, 5xxx and 6xxx series, the large cathodic particles are predominantly Fe-containing. A Zr-based conversion coating was found not to uniformly cover the surface of AA1050, but the oxide deposition was concentrated on and around IMPs containing mainly Fe and Si.<sup>58,64</sup> Most studies were carried out on AA6xxx series (Table III). In 6xxx alloys, the nucleation and growth of Zr/Ti oxide amorphous layer occurs on and around the most abundant intermetallic particles,  $\alpha\text{-(Fe,Mn)}_3\text{SiAl}_{12}$ , which act as cathodic sites.<sup>94,105,107</sup> Deposition is initiated when the natural oxide layer is removed by the etching action of fluoride ions. The film grows laterally surrounding these cathodic sites, progressively covering the entire surface, but is always thicker at the IMPs. Full coverage of the substrate could not be achieved at a pH of 2.9.<sup>95</sup> When coated at pH 4.0, the coating extended over a broader area around the particles and over the surface.<sup>95</sup> Once the IMPs were covered with deposits, the cathodic activity was diminished.<sup>94,105</sup> The Volta difference between IMPs and matrix was reduced and eventually eliminated completely at longer deposition times (300 s) (Fig. 3).<sup>107</sup>

In 2xxx series, the Cu-containing IMPs are the preferential sites of cathodic process where the subsequent precipitation of Zr/Ti-rich deposits initiates.<sup>106</sup> Cu-rich IMPs are porous due to dealloy-

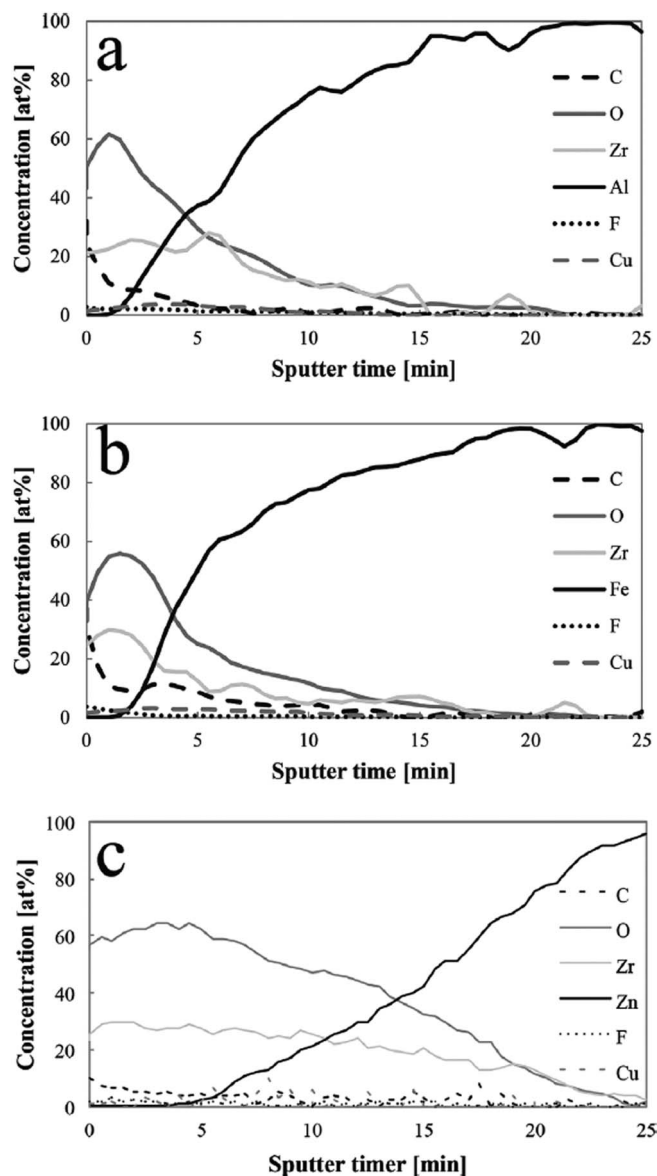


**Figure 7.** AES depth profiles of Zr-based conversion films on (a) AA6014, (b) cold rolled steel, and (c) hot dip galvanized steel deposited during 90 s of immersion in conversion bath with stirring. Reprinted from the publication by J. Cerezo, R. Posner, I. Vandendael, J.H.W. de Wit, H. Terryn, and J.M.C. Mol, *Mater. Corros.*, **67**, 361–367 (2016) with permission from Wiley and Sons.<sup>108</sup>

ing of the other intermetallic elements during the deoxidation step (i.e. dissolution of Al, Mg, etc.). Near the Cu-rich sites, the Zr coating appeared thicker and extended more toward the AA2024-T3 matrix.<sup>112</sup>

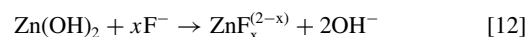
In 7xxx series, the potential difference between the Cu-containing IMPs and matrix was found to be the driving force for the initiation of the cathodic reaction and subsequent deposition process.<sup>74</sup> The deposition varied along the particles, being intensified in their center and then decreased toward the particle peripheries. After deposition of a conversion coating, the Volta potential difference between Cu-rich IMPs and the surrounding matrix decreased, indicating reduced corrosion activity at the surface.

**Galvanized steel.**—The various zinc- or zinc-alloy-coated steels (hot dip galvanized, electroplated, electrogalvanized) used as substrates for conversion coatings are listed in Table III. The process of zinc corrosion in Ti- or Zr-conversion baths is a combination of anodic zinc dissolution, and cathodic hydrogen evolution or oxygen reduc-

**Table III.** Literature studies of conversion coatings on various substrates.

Substrate	Reference
<b>Al and Al alloys</b>	
Al	19,33,40,49,77
AlMg0.5	83
Al-Cu alloys	49
Al-Mg alloys	137
AlMg0.5Si0.4	95
$\alpha$ -Al(Fe,Mn)Si, AlMg0.5Si0.4	94
AA1050	47,58,64,87,90,91
AA2024	40,74,75,81,84,92,106,112,128
AA3003	41,44,45,139
AA5005	29
AA5083	30
AA5182	45
AA6014	85–88,104
AA6016	107,108
AA6060	94,95,105,124
AA6061	89,93,112,136
AA6063	42,50,53,59,61,69,70
AA7075	74,112
AA8021	110
<b>Multi-metal surfaces</b>	
AA3003, HDG steel	41
Al alloys, steels, galvanized steels	111
AA6014, HDG steel, CR steel	85
AA6016, CR steel, HDG steel	108
Al, Zn, Mg	135
<b>Zn and Zn or Al coated steels</b>	
HDG and Galfan steel	43
HDG steel	31,34,52,72,113
Electrogalvanized / electroplated steel	32,35,48,68,78,79
Zn galvanized steel	54
HD Al-Si coated steel	102
Zn-Al-Mg alloy coated steel	55
Zn	51,62
<b>Cold rolled, low carbon and mild steels</b>	
Cold-rolled steel	6,57,67,82,96,97,119
Carbon steel	57
Low carbon steel	63,125
Mild steel	65,67,98,99,138
<b>Magnesium alloys</b>	
AZ31	80,101,140
AZ50	39,109
AM60	38,71,140
AM60B	100
AZ91	36,37,39,60,109,140

tion, which is the rate determining process.<sup>49</sup> During the initial stage of conversion layer formation, the primary zinc layer is etched and replaced by a thin Zr-based oxide/hydroxide layer.<sup>34</sup> Hydrogen evolution occurs and hydrated oxides of Zr, Ti and Zn form, accompanied by HF and H<sub>2</sub> evolution. HF can dissolve Zn and ZnO to form ZnF<sub>2</sub>.<sup>48</sup> Native Zn oxide layer can also be dissolved by “free” hexafluorides or fluorides:<sup>52</sup>



Zinc was identified in the conversion layer as ZnO,<sup>32,48,52</sup> Zn(OH)<sub>2</sub>,<sup>31,34,113</sup> and ZnF<sub>2</sub>.<sup>48,51</sup> Zn(OH)<sub>2</sub> is more protective than ZnO due to its lower electronic conductivity.<sup>126</sup> The amount of ZnO/Zn(OH)<sub>2</sub> in the interfacial layer between substrate and conversion layer was reported to be between 5 and 10 at.%.<sup>31,34</sup> An example of a depth profile of a Zr-based coating formed on HDG steel is presented in Fig. 7c.<sup>108</sup> ZnO was enriched at the inner interface with the base Zn metal, followed by predominant formation of Ti- and Zr-oxide/hydroxides also incorporating ZnF<sub>2</sub>.<sup>48</sup>

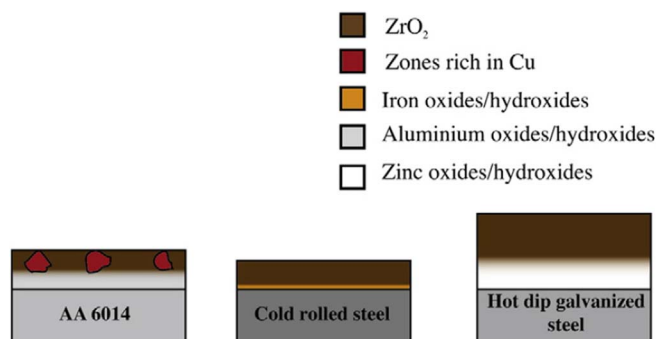


**Figure 8.** Schematic drawing of Zr-based conversion layers on different substrates. Reprinted from the publication by J. Cerezo, I. Vandendael, R. Posner, K. Lill, J.H.W. de Wit, J.M.C. Mol, and H. Terryn, *Surf. Coat. Technol.*, **236**, 284–289 (2013) with permission from Elsevier.<sup>85</sup>

The formation of Zr-based conversion coatings affects the Volta potential difference between Zr oxide and zinc base metal, causing a cathodic shift.<sup>34</sup> Zr-based conversion coatings deposited on Zn-Al alloy coated steel sheets were investigated by SKP and field emission scanning electron microscopy with energy dispersion X-ray spectroscopy (FE-SEM/EDS).<sup>55</sup> This alloy contains a primary Zn phase, an Al rich phase and a binary eutectic MgZn<sub>2</sub>-Zn phase. The Zn-rich phases are the most noble while the Al-rich phases are less noble; both are more noble than Mg-rich phases. Upon immersion in conversion bath containing H<sub>2</sub>ZrF<sub>6</sub> for short times (up to 40 s), the deposition started preferentially at the Zn-rich phases, which acted as local cathodes. Simultaneously, the Al- and Mg-rich phases underwent anodic dissolution leading to their enrichment with Zn. Upon longer immersion, i.e. when conditions of local alkalization were achieved, the coating also precipitated on the Mg-rich phases.

**Steels.**—XPS spectra of untreated and H<sub>2</sub>ZrF<sub>6</sub>-treated low carbon steel substrate revealed that the untreated steel was covered by Fe<sub>2</sub>O<sub>3</sub>.<sup>63</sup> After formation of Zr-based layer, the intensity of the Fe signal decreased but was still present, indicating that Fe was incorporated in the ZrO<sub>2</sub> coating. An example of a depth profile of Zr-based coating formed on cold rolled steel is presented in Fig. 7b.<sup>108</sup> Analogous to other substrates, the anodic reaction on CRS surface is dissolution of iron<sup>114</sup> and the cathodic oxygen reduction leads to conditions for precipitation of Zr hydroxide. The formation of FeF<sub>3</sub> was also reported.<sup>108</sup>

A schematic presentation of deposition of conversion coatings on different substrates, which summarizes the discussion presented above, is shown in Fig. 8.<sup>85</sup> Auger depth profiles of Zr-based coatings on Al and HDG steel show some interesting similarities and contrasts.<sup>41</sup> The treated HDG steel was richer in substrate elements, and poorer in the elements from the Zr conversion bath than the treated Al surface. In steel, the concentration of substrate elements was relatively constant throughout the coating, whereas they gradually increased toward the substrate for Al. This difference was ascribed to a more diffuse interface on Zn-coated steel than on Al, leading to greater coating laminar differentiation. This may be related to the effect of different ionic and electronic conductivities of the substrate metal oxide.<sup>85</sup> The increase in conductivity enhances the anodic dissolution reactions and, consequently, coating thickness, which was the greatest for HDG steel and the smallest on the Al alloy (Figs. 7 and 8). Note that this is different than what was found for pure metals, as mentioned above.

### Characteristics of Conversion Coatings

The role of the cathodic reaction in the deposition mechanism of Zr/Ti-based conversion coatings suggests that there could be large

variations of coating composition, morphology and thickness depending on the conditions. This will be discussed in the current section.

**Composition.**—The composition of conversion coatings is strongly dependent on the conversion bath composition, including additives, as well as the type of substrate and its surface chemistry. These effects were already discussed in detail above. Only the first issue, i.e. the effects of the primary composition of the conversion bath, the Ti and Zr contents, will be discussed.

Most commercial fluoro-based conversion baths are mixed in that they contain both Zr and Ti compounds (Table II). The resulting coatings contain a mixture of Zr and Ti oxides, as well as fluorides, phosphates, and other organic and inorganic compounds depending on the bath composition.<sup>90,94,95,105,106,127</sup> When commercial baths contain trivalent chromium, the coating also contains Cr.<sup>84,127</sup> The Zr-based TecTalis coating was found to contain Zr and O at a ratio corresponding closely to stoichiometric ZrO<sub>2</sub>.<sup>6</sup>

Among non-commercial conversion baths discussed in the literature, more variations in composition and ratio between reagents are found (Table I). Ti was present in the coating mainly as oxide/hydroxide but also as fluoride, and other compounds such as phosphate, carbonate, etc., depending on the conversion bath additives.<sup>31,41</sup> The source of Ti strongly affects the coating formation and its characteristics.<sup>73</sup> Coatings obtained from a TiCl<sub>4</sub> bath had better uniformity but the growth rate was more than two times slower than coatings obtained from H<sub>2</sub>TiF<sub>6</sub> because of faster surface activation by fluoride than chloride ions. The smaller covalent and van der Waals radius of F<sup>−</sup> in comparison to Cl<sup>−</sup> results in a higher charge density for F<sup>−</sup>, which promotes faster surface activation than Cl<sup>−</sup>.<sup>40,73</sup> TiCl<sub>4</sub>-based conversion coatings on CRS that were subsequently coated with epoxy exhibited better corrosion and adhesion performance than samples with H<sub>2</sub>TiF<sub>6</sub>-based conversion coatings, indicating that the former had better uniformity but required more time to be achieved.

Mixed Zr/Ti-based conversion coatings were investigated in several reports.<sup>29,46,48,50,54,59,61,69,70,74,76,107</sup> Some formulations contained more Ti,<sup>50,59,69,70</sup> whereas others contained more Zr.<sup>48,60,74,76,127</sup> Even when the ratio of Ti and Zr compounds in the bath was reported, it is difficult to find a relationship between their concentration in the bath and their content in the coating. When both compounds were present in the bath, both were also usually found in the coating<sup>46,48,59,69,70</sup> but not necessarily in the same ratio as in the bath.<sup>46,48,50</sup> In Zr-based coatings, Zr was present mainly as ZrO<sub>2</sub><sup>49,55</sup> or as ZrO<sub>2-x</sub>(OH)<sub>2x</sub>·nH<sub>2</sub>O.<sup>38</sup> In some studies, fluoride was detected within the coating,<sup>30,34,36,40,46,49,51,52,75</sup> and in other studies it was not detected.<sup>55,58,63</sup>

The concentration of H<sub>2</sub>ZrF<sub>6</sub> and H<sub>2</sub>TiF<sub>6</sub> in the conversion bath affects the Zr and Ti concentration in the coating, but also the concentration of F in the coating. Increasing the concentration of H<sub>2</sub>ZrF<sub>6</sub> from 0.001 M to 0.1 M in conversion baths resulted in decreased Zr coating content from 10 to 1.3 at.%.<sup>38</sup> Similarly, for a H<sub>2</sub>TiF<sub>6</sub> conversion bath, the highest Ti content was obtained was obtained at a concentration of 0.0001 M.<sup>38</sup> The decrease in Ti or Zr concentration in the layer deposited from more concentrated baths was accompanied by increased concentration of F. These changes in coating composition are related to the lower pH of more concentrated solutions and the fact that at higher concentration the fluoride ions became too aggressive toward the substrate and thus detrimentally affect the layer formation.<sup>38,71</sup> Low H<sub>2</sub>ZrF<sub>6</sub> and H<sub>2</sub>TiF<sub>6</sub> concentrations favor the formation of a protective Zr- and Ti-layer. Optimal corrosion performance was noticed at a concentration of 100 mg/L H<sub>2</sub>ZrF<sub>6</sub><sup>58</sup> and 0.01 M H<sub>2</sub>ZrF<sub>6</sub>.<sup>67</sup>

**Morphology and thickness.**—The coating morphology when analyzed by SEM follows the morphology of underlying, pre-treated substrate, but exhibits a somewhat less rough appearance.<sup>47,53,64,77,83,104</sup> The coatings have globular structure with nanometer-sized particulates.<sup>30,40,42,46,48,50,56,58,61,74,76,77,95,97,98,114</sup> The deposit at inter-metallic particles is thicker, compared to the rest of surface.<sup>88,95,105,107</sup>



The coating may be non-uniform due to the fact that it starts at IMPs in Al alloys or different phases at the surface of steels, and then spreads across the surface.<sup>38,58,71,74,102,105,106</sup> After sufficient immersion time (Figs. 3 and 4) the coating covers the surface uniformly on Al alloys,<sup>69,81,107,112</sup> HDG steel,<sup>52,68,72</sup> and CRS.<sup>6,73,82,96,97</sup> In some cases, the coatings have not covered the surface uniformly even after prolonged immersion because the coating coarsens.<sup>89,37,60</sup>

Cracks were observed at the coating surface, especially after long immersion times. Cracks can form during exposure to the vacuum of an SEM chamber because of dehydration and shrinkage, but also can form before introduction into the SEM vacuum during exposure in dry air<sup>49,52,69,79,80,94,96,106,127</sup> or during a curing step at 70°C.<sup>107</sup> Cracking was also observed in coatings deposited in conversion baths of higher temperature (40°C).<sup>97</sup> The addition of Ce to Zr-based coatings on AA2024 induced submicron cracks that reached the substrate surface, which may account for the coating self-healing ability.<sup>81</sup>

The majority of Zr/Ti based conversion coatings are in the category of thin coatings, between 10 nm and 50–80 nm.<sup>6,32–34,44,49,52,76,77,88,90,91,97,102,105,106,108,112</sup> Coatings with thickness between 100 nm and 600 nm were reported as well,<sup>48,81,94,127</sup> and even in the micrometer thickness range from 1.0  $\mu\text{m}$  up to 6  $\mu\text{m}$ .<sup>30,37,43,59,61,80,119,127</sup> Thickness is related to other parameters such as substrate, pH, time of immersion and stirring, as discussed in Conversion bath parameters and Effect of substrate on coating formation sections.

As mentioned above, the coating deposition starts at the inter-metallics and progressively grows on and around them eventually covering the entire surface, so the coating is considerably thicker at the IMPs, as indicated by SEM/EDS profiles and mapping and Auger spectroscopy.<sup>94,108</sup> This is different from chromate coatings, which are formed by redox reaction of hexavalent chromium from the solution at the surface and are thicker at the matrix and thinner at IMPs.<sup>94</sup>

### Corrosion Performance of Conversion Coatings

The mechanism of coating formation and the subsequent properties of the coating such as morphology, composition and thickness are dependent on the substrate (Effect of substrate on coating formation section). Consequently, corrosion performance is dependent on type of substrate and type of coating. A large variety of performance was observed for Ti/Zr conversion coatings, ranging from poor to excellent. These are presented in this section separately for Al alloy, galvanized steel and steel substrates and for Ti-, Ti/Zr- and Zr-based coatings. Generally, the presence of coatings caused an increase in polarization resistance,  $R_p$ , reduction of cathodic and, especially, anodic current density accompanied by a shift of corrosion potential,  $E_{\text{corr}}$ , and establishment of passive behavior in the anodic part. In electrochemical impedance spectroscopy (EIS) spectra, an increase of diameter of the capacitive loop and increase in impedance in the low frequency region were observed.

**Aluminum alloys.**—The corrosion performance of Ti-, mixed Ti/Zr- and Zr-based coatings on aluminum alloys differs depending on the type of coating and substrate. Furthermore, additives to conversion bath can greatly affect the final performance. Ti-based coatings were investigated on Al 5005,<sup>77</sup> AA3003<sup>44</sup> and AA6014<sup>104</sup> and showed limited protection, although improved adhesion of a subsequent organic coating was observed on Al 5005.<sup>77</sup>

Mixed Ti/Zr-based commercial coatings did not provide strong protection of Al alloys. The Gardobond coatings X4707 (Ti/Zr) were not efficient for AA6060.<sup>94,95</sup> Similarly, Bonderite M-NT 5200 (Zr/Ti-based) provided almost no protection for AA2024 substrate, which was ascribed to non-uniformity or defects in the coating.<sup>106</sup> Alodine 5700 (Ti/Zr based) deposited on AA2024-T3 had unacceptable performance in the ASTM B117 salt spray test (less than 200 h) and marginal performance in the GM 9540P accelerated corrosion test.<sup>84</sup> Alodine 4830 (Ti- or Zr-based) coatings deposited on AA6061 achieved optimal corrosion performance when deposited at pH 4.5 for

90 s.<sup>89</sup> However, the protection was limited during 24 h immersion in 3.5 wt% NaCl. Under the same conditions, chromate coatings remained protective.

Various mixed Ti/Zr non-commercial coatings showed a greater ability to protect Al alloys. When containing different additions such as tannic acid,<sup>50,59,70,76</sup> Mo,<sup>74</sup> Mn<sup>61,74</sup> and phosphates,<sup>30</sup> better performance was achieved than for Ti-based coatings. The additions of Mo and Mn were beneficial for corrosion resistance in an  $\text{Na}_2\text{SO}_4 + \text{NaCl}$  solution for Zr/Ti coatings deposited on AA2024 and, especially, on AA7075 (Fig. 9a).<sup>74</sup> Good performance of mixed Ti/Zr-based coatings was also found on AA6063-T52<sup>42,50,61</sup> and AA6016.<sup>107</sup> Excellent performance was reported for Zr/Ti-coatings containing tannic acid and metavanadate deposited on AA6063.<sup>59,70</sup> When coated, the  $E_{\text{corr}}$  in aerated NaCl solution shifted more positive by 430 mV, and  $i_{\text{corr}}$  was reduced from 7.5 to 0.6  $\text{mA cm}^{-2}$  (Fig. 9b).<sup>70</sup> Accelerated testing showed superior corrosion performance of the coating compared to uncoated alloy and commercial chromate coating (DCHZ-405).<sup>70</sup> After 72 h, many white corrosion products were observed on uncoated AA6063, indicating severe corrosion.

Zr-based coatings showed better performance compared to Ti coatings. For AA1050, good electrochemical results were achieved for Zr-based coatings containing PAA and PAM in that they exhibited constant capacitance during more than 50 days exposure to 3.5% NaCl.<sup>47</sup> When tested in a salt spray chamber for 1000 h, however, these coatings performed worse than commercial chromate coatings.<sup>47</sup> Zr-based coating containing phosphate deposited on AA5083 exhibited much better corrosion performance than that of commercial Cr-free treatments and close to that of commercial chromate coatings (Fig. 9c).<sup>30</sup> Both cathodic and anodic processes were retarded on the Zr coating, and the extent of the passive range was broader for the Zr conversion coating than for CCC. When tested in a salt spray chamber for 1500 h, Zr-coating performed slightly worse than commercial CCC but better than Cr-free coating.

NCP Zr/Zn conversion coatings from NAVAIR were tested on AA2024-T3, AA6061-T6 and AA7075-T6.<sup>112</sup> The coating shifted the  $E_{\text{corr}}$  in the positive direction by about 250 mV, suppressed anodic currents more than cathodic currents around  $E_{\text{corr}}$  by at least a factor of 10  $\times$ , and shifted the pitting potential in the noble direction (Fig. 9d). The coating also provided excellent corrosion protection to AA2024-T3, AA6061-T6 and AA7075-T6 alloys during a 14-day full immersion test in  $\text{Na}_2\text{SO}_4 + \text{NaCl}$ . However, during neutral salt spray and thin-layer mist tests, the NCP provided little stand-alone protection to the Al alloys and was inferior to a TCP coating. After a 1-week beach exposure, NCP coatings on AA2024-T3, AA6061-T6 and AA7075-T6 showed greater levels of pitting, spotting and surface damage than TCP coatings. These results demonstrated that electrochemical evaluation under immersion conditions does not always reflect coating performance during accelerated degradation or environmental exposure.<sup>112</sup> It was reported recently that PreCoat A32 coating consisting of Zr(IV), Cr(III) and fluorides achieved similar performance in a 168 h salt spray test as Alodine 1200 CCC, indicating that it is a promising alternative for aeronautic and aerospace industries.<sup>128</sup>

Self-repair ability was studied in several reports. Vanadate-containing Zr-based coatings on AA6063 promoted self-healing as indicated by EIS spectra in 3.5% NaCl.<sup>53</sup> Without  $\text{Ce}(\text{NO}_3)_3$ , Zr-based conversion coating deposited on AA2024 improved the corrosion resistance only to a limited extent. However, when  $\text{Ce}(\text{NO}_3)_3$  was added, the long-term results were greatly improved.<sup>81</sup> The self-healing action of cerium was reflected in a continuous increase in charge transfer resistance during immersion (Fig. 6). When exposed to salt spray test for 168 h, the Zr-coating underwent heavy attack, whereas the Zr-Ce coating exhibited only surface discoloration after 168 h exposure with only few isolated pits, which was comparable behavior to chromate coatings.<sup>81</sup> A Zr-based coating containing Cr(III) on AA2024-T3 exhibited self-repair, as shown by EIS experiments in an artificial scratch cell.<sup>75</sup> The coating persisted up to 72 h salt spray chamber when corrosion products appeared.<sup>75</sup> Uncoated specimens showed corrosion after only 6 h of exposure.



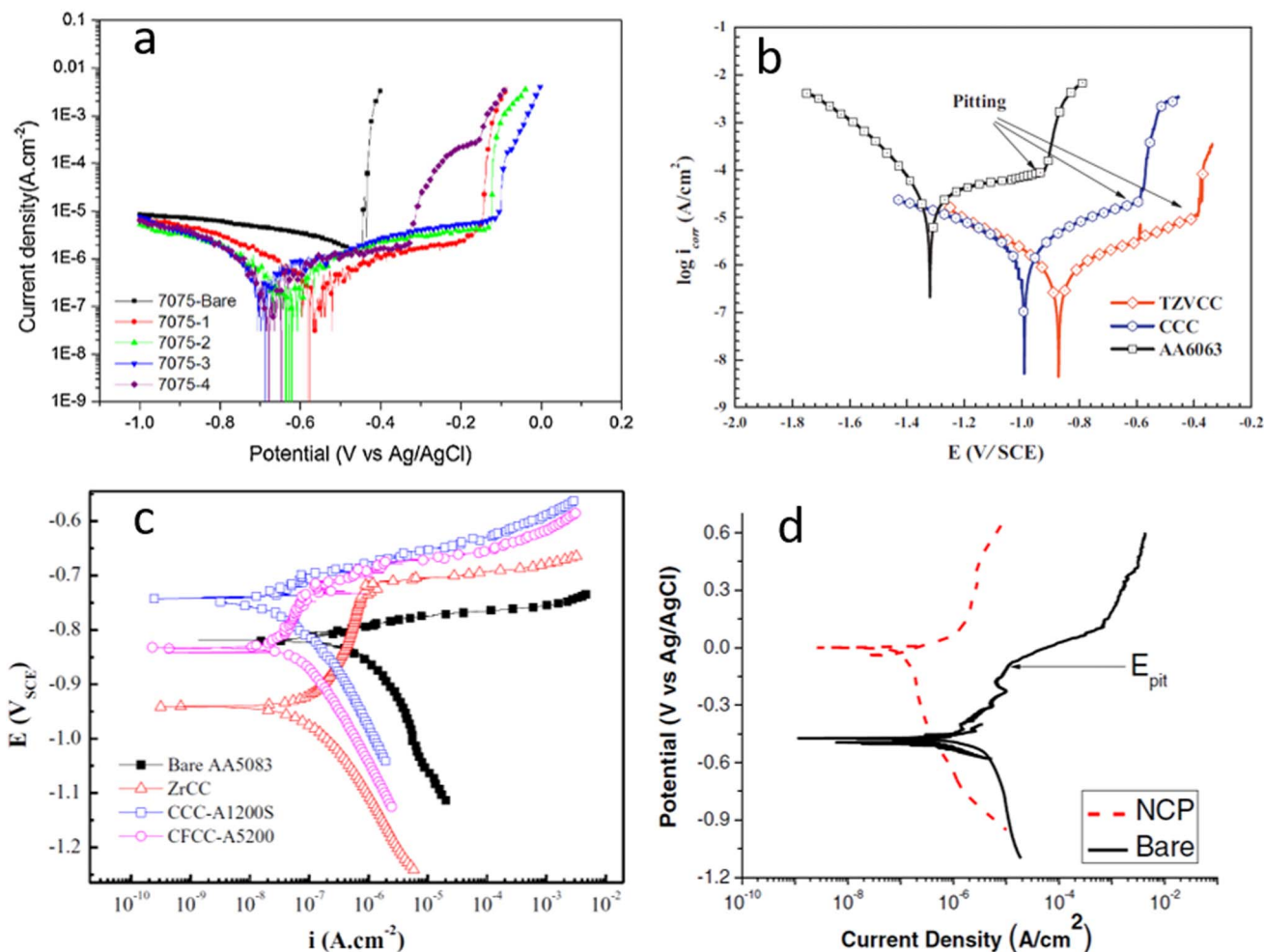


**Figure 9.** (a) Polarization curves of bare AA7075-T6 and coated using different Ti/Zr-based coatings: (1) 4 g/L  $K_2TiF_6$ +6 g/L  $K_2ZrF_6$ +20 g/L  $NaMoO_4$ +20 g/L  $KMnO_4$ , (2) 8 g/L  $K_2ZrF_6$ +20 g/L  $NaMoO_4$ +20 g/L  $KMnO_4$ , (3) 20 g/L  $NaMoO_4$ +20 g/L  $KMnO_4$ , (4) 8 g/L  $K_2TiF_6$ +20 g/L  $NaMoO_4$ +20 g/L  $KMnO_4$  in 0.1 M  $Na_2SO_4$  + 10 mM NaCl solution. Reprinted from the publication by P. Santa Coloma, U. Izagirre, Y. Belaustegi, J.B. Jorcin, F.J. Cano, and N. Lapeña, *Appl. Surf. Sci.*, **345**, 24–35 (2015) with permission from Elsevier.<sup>74</sup> (b) Polarization curves of bare AA6063 and coated using commercial chromate coating (CCC) and Ti/Zr-V-based coating in 3.5 wt% NaCl solution. Reprinted from the publication by W. Zhu, W. Li, S. Mu, N. Fu, and Z. Liao, *Appl. Surf. Sci.*, **405**, 157–168 (2017) with permission from Elsevier.<sup>70</sup> (c) Polarization curves of bare AA5083 and coated using commercial chromate coating (Alodine 1200S), commercial non-chromium coating (Alodine 5200) and Zr-based coating containing phosphate in 3.5 wt% NaCl solution. Reprinted from the publication by Y. Liu, Y. Yang, C. Zhang, T. Zhang, B. Yu, G. Meng, Y. Shao, F. Wang, and L. Liu, *J. Electrochem. Soc.*, **163**, C576–C586 (2016) with permission from Electrochemical Society.<sup>30</sup> (d) Polarization curves of NCP-coated and uncoated (bare) AA2024-T3 specimens in naturally-aerated 0.5 M  $Na_2SO_4$  + 0.1% NaCl. Reprinted from the publication by L. Li, B.W. Whitman, C.A. Munson, R. Estrada, C.A. Madzdzor, and G.M. Swain, *J. Electrochem. Soc.*, **163**, C718–C728 (2016) with permission from Electrochemical Society.<sup>112</sup>

Summarizing, some Ti/Zr and Zr-based coatings containing various additives achieved exceptional performance on aluminum alloys. For example, Ti/Zr-based coatings containing metavanadate and tannic acid on AA6063 showed better results in a salt spray chamber than CCC,<sup>59,70</sup> whereas a Zr-based coating containing phosphate on AA5083 exhibited results similar to CCC.<sup>30</sup> Further improvements are required for some coatings. For example, Zr-based coatings containing Mo and Mn on AA2024 and AA7075 showed excellent electrochemical results but salt spray results were still worse than CCC.<sup>74</sup>

**Galvanized steels.**—Ti-, Zr-based and mixed TiZr coatings were investigated on galvanized steels. Ti-based coatings on galvanized steel prepared from  $TiCl_4$  and  $H_2SiF_6$  exhibited much larger impedance compared to chromate coating and uncoated substrate and developed less white rust when tested in a salt spray chamber for 240 h.<sup>35</sup> Similarly, coatings based on  $TiCl_3$  and  $H_2SiF_6$  deposited on Zn electroplated steel were superior to chromate coatings (Fig. 10a).<sup>79</sup> Even after 216 h of salt spray, no signs of zinc corrosion were observed. A Ti-based coating prepared from baths containing  $H_3PO_4$ ,

$Mn_3(PO_4)_2$  and organic phase,<sup>31,72</sup> and  $Mn(NO_3)_2$  and  $H_3PO_4$ <sup>32</sup> on HDG steel resulted in about one order of magnitude smaller  $i_{corr}$  and a slight positive shift of  $E_{corr}$  in 3.5% NaCl.<sup>31,72</sup> When using another Ti-based coating on Zn-coated steel, zinc corrosion products appeared on only 5% of the surface, whereas uncoated HDG steel was severely corroded.<sup>32</sup>

Two types of mixed Ti/Zr coatings were tested on galvanized steels and showed relatively good performance.<sup>48,54</sup> Good results were also reported for a commercial Zr-based coating (Bonder D 6800) developed in 1990s<sup>43</sup> and recently for Zr-based coatings containing Cu or Fe on HDG steel.<sup>52</sup> Zr-based coatings with different additives have been investigated. When Ni ions were present in a Zr conversion bath, the corrosion performance was not improved in comparison to the Zr-based coating without Ni (Fig. 10b).<sup>68</sup> However, when a Ni coating was formed on top of a Zr-based coating, superior performance was achieved. During immersion in  $NiSO_4$  solution, a more resistive and uniform coating was formed.

Cathodic and anodic polarization curves were measured in 0.5 M NaCl for hybrid coatings with a Zr-rich inorganic matrix containing

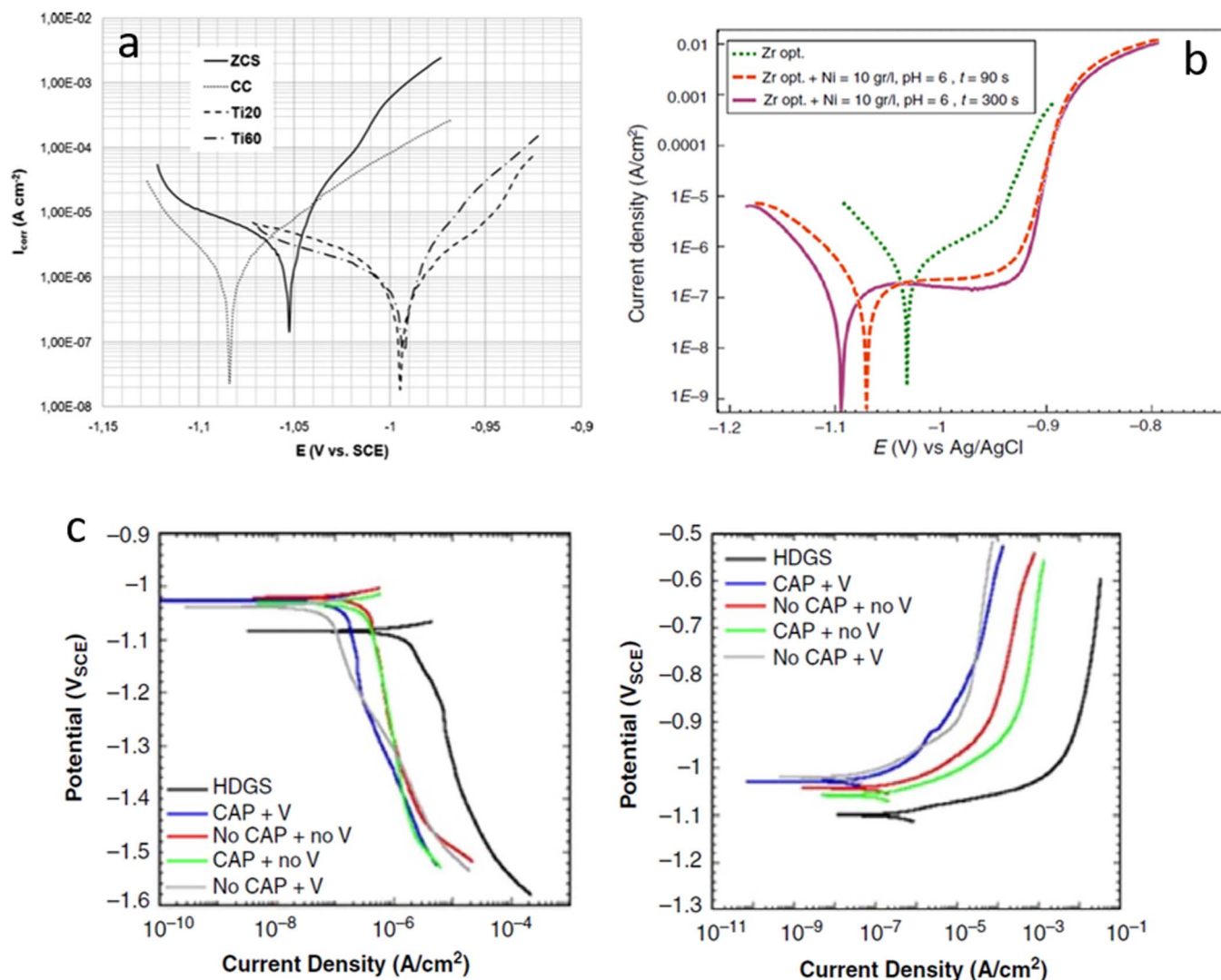


**Figure 10.** (a) Polarization curves of bare Zn electroplated steel and coated using commercial chromate coating (CC) and Ti-based coatings prepared from  $\text{TiCl}_4$  and  $\text{H}_2\text{SiF}_6$  in non-aerated 0.5 M NaCl solution. Coatings were prepared with two time of immersion 20 s (Ti20) and 60 s (Ti60). Reprinted from the publication by B. Szczygieł, J. Winiarski, and W. Tylus, *Mater. Chem. Phys.*, **129**, 1126–1131 (2011) with permission from Elsevier.<sup>79</sup> (b) Polarization curves of bare Zn galvanized steel and coated using Zr-based coating post treated in  $\text{NiSO}_4$  (10 g/L, pH = 6) for 90 s and 300 s. Curves were recorded in 3.5 wt% NaCl solution. Reprinted from the publication by H.R. Asemani, A.A. Sarabi, H. Eivas Mohammadloo, and M. Sarayloo, *J. Coat. Technol. Res.*, **13**, 883–894 (2016) with permission from Springer.<sup>68</sup> (c) Cathodic (left) and anodic (right) polarization curves of uncoated hot dip galvanized steel (HDGS) sample and hybrid coated samples with different formulations measured in deaerated 0.5 M NaCl solution. CAP is cyclic-amine-containing polymer, V is vanadium. Reprinted from the publication by N.W. Khun, S. Adhikari, Y.Y. Li, G.S. Frankel, J. McGee, T. Smith, B. Bammel, and J. Zimmerman, *Corrosion*, **73**, 339–346 (2016) with permission from NACE.<sup>119</sup>

CAP organic polymer beads and V deposited on HDG steel.<sup>119</sup> The curves for coated samples were generally shifted to lower current densities with little change in  $E_{\text{corr}}$ , indicating protection by simple blocking of the surface (Fig. 10c). When the coating also contained vanadium, the current densities were lower, proving its beneficial effect.

Summarizing, some coatings containing additives like Mn and V exhibited good performance on galvanized steels and achieved performance similar to CCCs.<sup>35,79</sup> There are still possibilities for further improvement, especially in terms of additives and self-healing agents, as well as chemical post-treatment.

**Steels.**—Ti- and Zr-based coatings on steels were investigated. The corrosion resistance of Ti-based coatings deposited on CRS with various conversion parameters (time of immersion, pH, Ti concentration) were tested in 3.5 wt% NaCl.<sup>67,73</sup> The Ti source was  $\text{H}_2\text{TiF}_6$  or  $\text{TiCl}_4$ . Coatings obtained from  $\text{TiCl}_4$  achieved better uniformity and conse-

quently better corrosion resistance. Using optimized conversion bath parameters, the  $R_p$  increased, and  $i_{\text{corr}}$  decreased by approximately  $6\text{--}7 \times$ .<sup>73</sup>

$\text{TiCl}_4$ -based coatings containing  $\text{NiSO}_4$  or  $\text{MoO}_4$  were also tested on CRS in 3.5 wt% NaCl solution (Fig. 11a).<sup>82</sup> The significant improvement when Ni was added was ascribed to the formation of an outer layer of nickel, which acts as a physical barrier to inhibit the charge transfer and movement of ions. The detrimental effect of Mo was ascribed to the formation of a cracked Mo-based layer at the substrate/coating interface. Chemical post-treatment in  $\text{NiSO}_4$  solution increased the  $R_p$  about 80 times compared to uncoated steel and 50 times compared to TiNi-coated steel. This result points to further possibilities to improve corrosion performance of coated substrates, similar to what was observed for Zn galvanized steel.<sup>68</sup>

Commercial Bonderite NT-1 Zr-based coatings on CRS shifted the  $E_{\text{corr}}$  more positive by 200 mV and reduced  $i_{\text{corr}}$  2–3 x compared to uncoated steel in 3.5 wt% NaCl.<sup>96,97</sup> In contrast, it was reported that

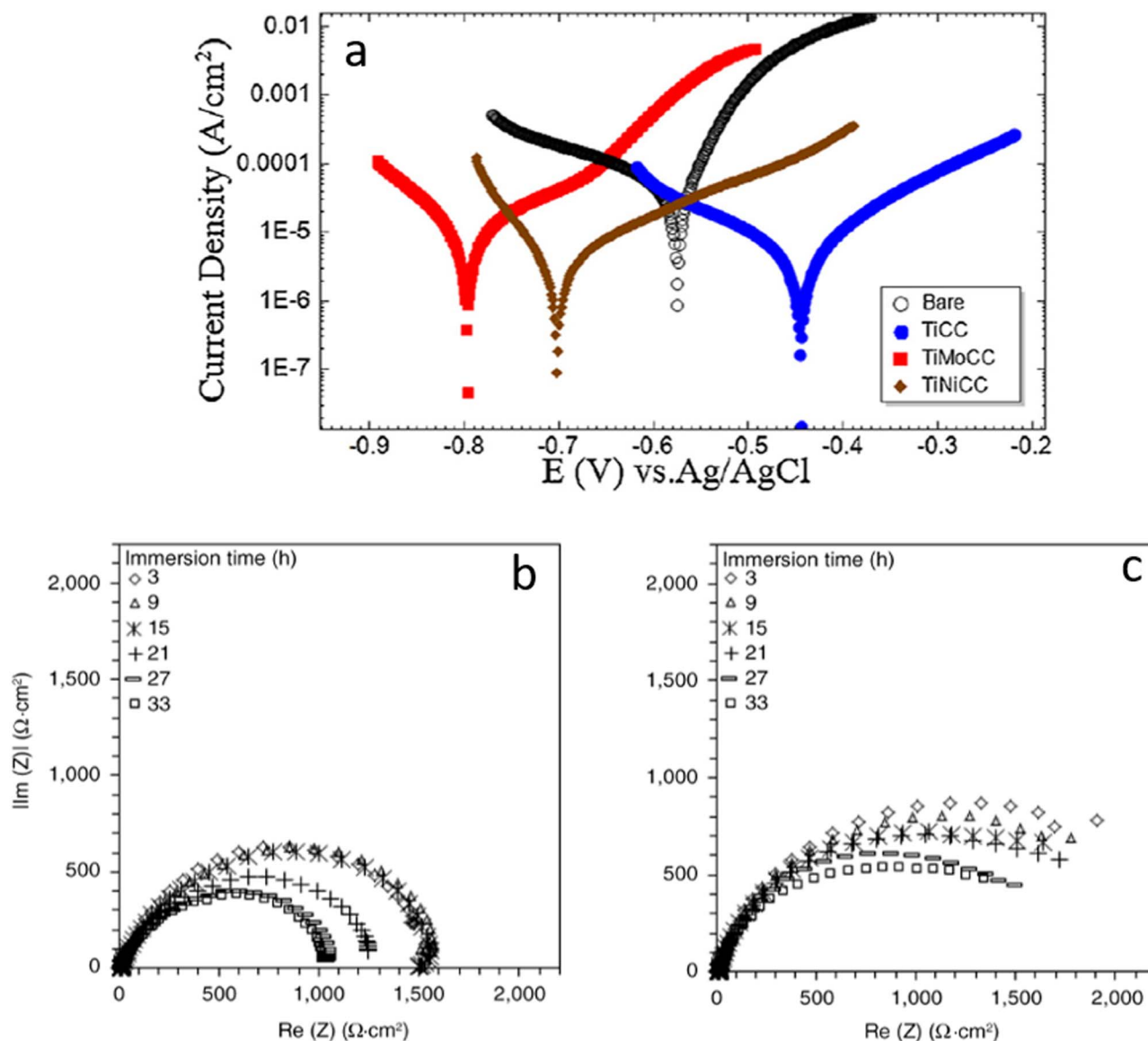


**Figure 11.** (a) Polarization curves of bare cold rolled steel and coated using Ti-, TiMo- and TiMoNi-based coatings in 3.5 wt% NaCl solution. Reprinted from the publication by H. Eivaz Mohammadloo, and A.A. Sarabi, *Appl. Surf. Sci.*, **387**, 252–259 (2016) with permission from Elsevier.<sup>82</sup> (b) Nyquist plots of untreated steel substrate and (c) pre-treated steel substrates in a hexafluorozirconium acid-based solution for 120 s measured in neutral 0.5 M Na<sub>2</sub>SO<sub>4</sub> solution as a function of immersion time. Reprinted from the publication by N.W. Khun, and G.S. Frankel, *Corrosion*, **71**, 277–284 (2015) with permission from NACE.<sup>125</sup>

Bonderite NT-1 coatings when deposited on mild steel did not show any substantial improvement of corrosion characteristics compared to the uncoated substrate.<sup>98</sup>

Results published for Zr-based non-commercial coatings are diverse: Zr-based coatings containing MnSO<sub>4</sub> deposited on carbon steel in 3.5 %wt NaCl were similar to the uncoated samples, but with a smaller  $i_{\text{corr}}$  by approximately 2 x and a slight negative shift of  $E_{\text{corr}}$ .<sup>57</sup> Better performance of Zr-coated carbon steel was achieved in Na<sub>2</sub>SO<sub>4</sub>.<sup>125</sup> At longer immersion time in the conversion bath, the resistance increased due to the formation of a more uniform ZrO<sub>2</sub> layer (Fig. 11b). Similar results were obtained for low carbon steel<sup>63</sup> and mild carbon steel in NaCl solution.<sup>67</sup>

Summarizing, conversion coatings on steels achieved up to one order of magnitude smaller  $i_{\text{corr}}$  values and in most cases acted as barrier coatings, i.e. without changing the shape of polarization curves. Possibilities of long-term protection should be improved, presumably using additives or chemical post-treatments.

#### Adhesion Strength and Delamination Mechanism of the Substrate/Coating/Topcoat System

Corrosion resistance is not the only requirement for a surface treatment; the modified surface must bond to a subsequently applied organic layer and retain superior mechanical properties.<sup>41</sup> Clearly, a coating system cannot provide corrosion protection unless it remains adhered to the surface. When applied, conversion coatings are usually part of a full coating system, i.e. substrate, conversion coating, primer, and one or more topcoats. Organic coatings applied to conversion coatings are typically epoxy, but other polymers can also be applied, such as polyester, polyurethane, etc. Their thickness may range between 20 and 90 μm. Topcoats block ready access of electrolyte to the alloy surface. However, water can permeate through the organic coating, which can fail via underfilm corrosion leading to blisters and consequent loss of protection of the underlying matrix. Surface treatments such as conversion coatings are required to



promote adhesion of organic layers to the substrate and improve corrosion performance.<sup>93,129</sup>

The assessment of a pre-treatment on a substrate with no additional coating does not provide an indication of how the pre-treatment will perform as a part of a full coating system.<sup>84</sup> Two related processes are important: adhesion and cathodic delamination. In addition to dry adhesion, i.e. adhesive bonding strength between conversion coating and organic topcoat usually measured by a pull-off method, wet adhesion strength following long-term immersion in an aggressive electrolyte should be tested. When corrosive protective coatings get physically damaged by impact, scratches or wear during service, the underlying substrate can directly contact the environment, and electrochemical reactions can take place at the coating/substrate interface.<sup>103</sup> Anodic dissolution of the substrate can then take place in defect areas, which releases electrons to cathodic sites beneath the coatings where oxygen is reduced and hydroxyl ions are produced ( $O_2 + 2H_2O + 4e^- \rightarrow 4OH^-$ ). A buildup of  $OH^-$  ions under coatings can result in alkalization, which then weakens the adhesion between coating and substrate. This process is followed by the transport of cations along the interface between the anodic defect and cathodic end. This process, which is termed cathodic delamination, is recognized as one of the primary mechanism of coating failure on steel.<sup>129–133</sup> Cathodic delamination dramatically decreases with increased surface roughness of the underlying steel substrate, as shown by the SKP technique.<sup>103</sup> Adhesion strength of the conversion coating is dependent on the substrate pre-treatment, as shown by blister test for acetoacetate coatings on various conversion coatings on AA2024-T3.<sup>134</sup>

**Aluminum alloys.**—Different topcoats on Al alloys have been tested, including polyester,<sup>41,104</sup> acrylic,<sup>41,107</sup> and epoxy.<sup>30,47,58,64,69,70,77,93,95</sup> A Zr-based coating on AA1050 enhanced the pull-off adhesion of an epoxy topcoat.<sup>58</sup> This was ascribed to increased surface roughness and surface energy, which promote wettability of the substrate and stronger adhesive bonds.<sup>64</sup> Dry and recovery adhesion (after 20 days immersion in 3.5 wt% NaCl) were measured by the pull-off adhesion test. Adhesion loss was calculated according to:

$$\text{adhesion loss (\%)} = \left(1 - \frac{\text{recovery adhesion}}{\text{dry adhesion}}\right) \times 100\% \quad [13]$$

The dry adhesion strength of epoxy topcoat applied on a Zr-coated sample was higher than that measured on a chemically treated uncoated substrate. The adhesion loss was the lowest for the Zr-coated sample. Excellent adhesion was reflected also in high corrosion performance during 60 days immersion in 3.5 wt% NaCl.<sup>64</sup>

Conversion coating enhances corrosion resistance and increases paint adhesion by two mechanisms: (i) changing surface chemistry, and (ii) changing topography.<sup>64,134</sup> Increased wettability by increased surface energy for conversion-coated samples helps produce strong adhesion bonds with the organic coating through their polar groups. Most metal oxides, which are the main constituents of conversion coatings, can produce strong chemical bonding with highly polar groups of organic topcoats, like hydroxyls. A recent study showed that the bonding between Zr-conversion coatings on different metals and amide-functionalized molecules results from different bonding mechanisms: the increased surface hydroxide density after Zr-based coating on Al and Zn promotes Bronsted interactions, whereas Mg was characterized by fast Zr deposition kinetics accompanied by hydroxide removal.<sup>135</sup> Chemical bonding might not be sufficient for long-term high bond strength. Increased surface roughness by the conversion coating treatment enables the liquid applied organic coating to penetrate into the pores of the surface, thereby enhancing adhesion through mechanical interlocking. Adhesion strength increased with roughness due to an increase in area available for bonding at the primer/substrate interface, the tortuosity of path crack propagation, and an increase in plastic deformation.<sup>134</sup> Randomly abraded samples had higher adhesion strength than aligned abraded samples.<sup>134</sup>

Several examples of good performance of Al alloys with an organic topcoat have been reported: epoxy coated Zr-based coatings containing phosphate deposited on AA5083,<sup>30</sup> acrylic coated Zr/Ti-pre-treated AA6016,<sup>107</sup> polyester coated Ti-based silane coatings on AA6014<sup>104</sup> and epoxy coated Ti/Zr/V coating containing tannic acid on AA6063.<sup>69</sup> A Zr-treated (TecTalis 1800) AA6061-T6 substrate had higher resistance to moisture-induced corrosion than an untreated substrate, which was indicated by a smaller increase in roughness of the treated alloys with prolonged exposure to 99.5% relative humidity.<sup>93</sup> In situ atomic force microscope (AFM) scratching indicated that removal of an epoxy topcoat was more difficult for pre-treated substrates because of the enhanced adhesion strength.

**Galvanized steels.**—The propagation of corrosive de-adhesion of the organic lacquer on a Zr-based coating was dependent on the coating conversion times.<sup>34</sup> For shorter conversion time, oxygen reduction was impeded and the Volta potential was close to that of galvanized steel. Thus, a driving force for cathodic delamination did not exist. With increasing conversion time, propagation was faster due to the higher defect density of the conversion layer.<sup>34</sup>

The adhesion of an epoxy topcoat on Zr-based coating containing Ni and deposited on galvanized steel was investigated.<sup>68</sup> Bond strength was higher than for the bare sample. The addition of Ni to the Zr coating had a negative effect on the adhesion strength, but the highest adhesion strength was found when a Ni layer was deposited onto the Zr coating. This improvement was ascribed to enhanced surface roughness, which enabled mechanical interlocking between coating and topcoat.

**Steels.**—Mainly epoxy<sup>56,57,65,67,73,98,99,114,125</sup> and polyurethane<sup>63</sup> topcoats were tested on steels. A coating on CRS prepared from a  $TiCl_4$  bath exhibited higher adhesion strength to epoxy than that prepared from a bath containing  $H_2TiF_6$ .<sup>73</sup> Both exhibited higher strength compared to epoxy coating deposited on the bare CRS substrate.

Dry and wet adhesion properties of epoxy coated commercial Zr-based coatings on carbon steel were investigated (Fig. 12).<sup>99</sup> Although the impedance decreased with increasing exposure time (up to 250 h), there was no second time constant in the phase angle, which would indicate a change from capacitive to predominantly resistive behavior, as observed for uncoated substrate. Both dry and wet adhesion were higher than for untreated carbon steel even after 70 days exposure to 0.1 M NaCl. Similarly, good performance was achieved by TecTalis (Zr-based and Cu-containing) coated and painted (e-coat) CR steel samples up to 120 days immersion in 0.5 M NaCl.<sup>6</sup> High impedance values around  $1.4 \times 10^{10} \Omega \text{ cm}^2$  were measured. Pull-off tests, cathodic disbonding tests and EIS measurements indicated that a Zr-based coating on mild steel significantly improved adhesion of an epoxy topcoat.<sup>56</sup> The Zr coating increased the surface roughness (from 70 to 98 nm), which improved the adhesion of an organic topcoat and cathodic disbonding resistance as measured by EIS during 192 h in 3.5 wt% NaCl.

The additives to the conversion coating bath may be beneficial for corrosion resistance but can degrade adhesion. For example, the addition of  $Mn^{2+}$  ions improved the corrosion resistance of Zr-based coatings deposited on carbon steel, but the coating without  $Mn^{2+}$  showed the highest adhesion strength.<sup>57</sup> Therefore, while Mn may modify conversion coating characteristics, it cannot necessarily improve corrosion performance and adhesion in an organic coated system.

A polyurethane topcoat on TecTalis Zr-based coating lowered the cathodic delamination on low carbon steel.<sup>63</sup> Volta potential profiles of the uncoated carbon steel and epoxy-coated steel with different pre-treatment time in Zr-conversion bath are presented in Fig. 13.<sup>125</sup> Two potential levels characterize the SKP profiles: the lower potential on the left associated with the NaCl solution reservoir in the artificial defect and the higher potential of an intact coating on the right. When a coating delaminates from the substrate, the potential under the coating shifts toward the defect potential. The sharp change in potential marks the position of the end of the delamination zone, and the progress of cathodic delamination is reflected by the location of this potential



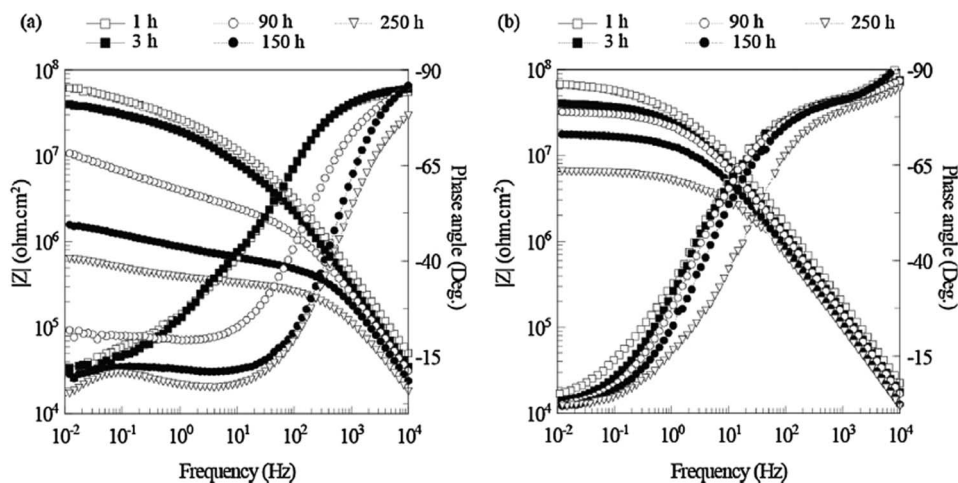


**Figure 12.** EIS spectra for (a) untreated carbon steel coated with fusion bonded epoxy and (b) Zr-treated carbon steel with fusion bonded epoxy after 1, 3, 90, 150 and 250 h of exposure to 0.1 M NaCl solution. Reprinted from the publication by M. Sababi, H. Terryn, and J.M.C. Mol, *Prog. Org. Coat.*, **105**, 29–36 (2017) with permission from Elsevier.<sup>99</sup>

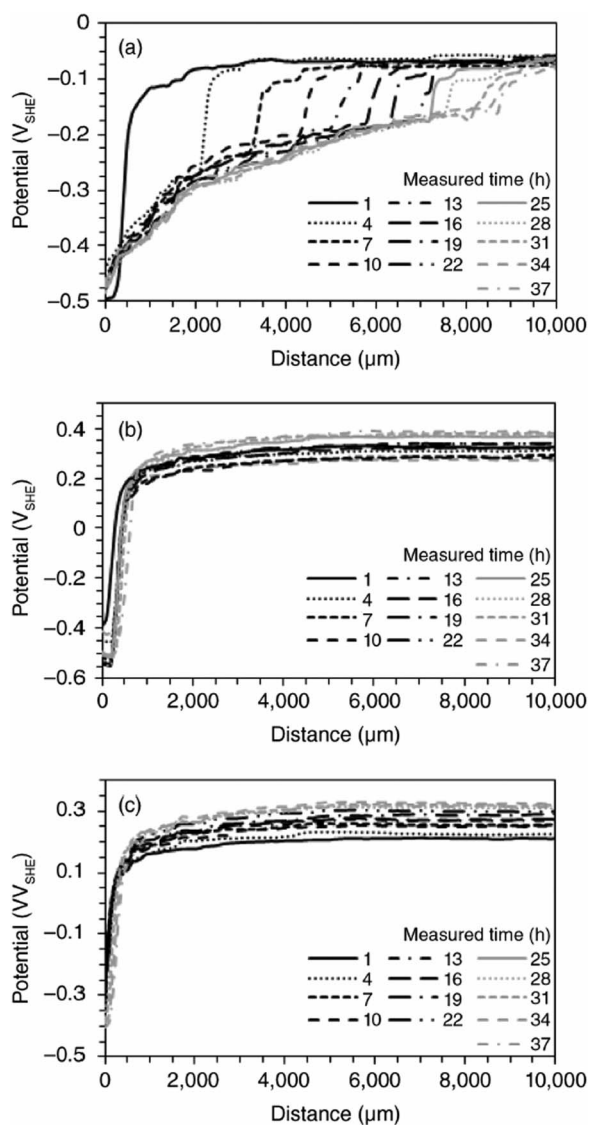


**Figure 13.** Scanning Kelvin Probe potential profiles of epoxy-coated steel samples with substrate surface pretreatment in a hexafluorozirconic acid-based solution for (a) 0, (b) 30, and (c) 120 s measured using SKP in neutral 0.5 M Na<sub>2</sub>SO<sub>4</sub> solution for different times as a function of distance. Reprinted from the publication by N.W. Khun, and G.S. Frankel, *Corrosion*, **71**, 277–284 (2015) with permission from NACE.<sup>125</sup>

jump with time. The average cathodic delamination rate decreased as a function of pre-treatment time. A decrease in pH resulted in a systemic decrease in the cathodic delamination rate of epoxy coating from untreated steel substrates via the decreased concentration of hydroxyl ions at the delamination front. When the steel was pre-treated using Zr-coating, this effect was not observed.

Summarizing, increased adhesion strength and reduced cathodic delamination are the most important benefits of Ti- and Zr-based conversion coatings. Some additives to the coating bath do not necessarily improve the adhesion strength, e.g. Ni and Mn, although they increase corrosion resistance. Therefore, the addition of additives should be optimized to improve both corrosion and adhesion performance.

### Concluding Remarks and Suggestions for Further Work

Conversion coatings based on Ti-, Ti/Zr- or Zr-oxides have already been partially implemented in automotive industry and have achieved good results on both ferrous and non-ferrous substrates. The advantages of these conversion coatings include their relatively simple and fast preparation method, the possibility of “dry-in-place” methodology, the low operation temperature, the avoidance of carcinogenic chromate compounds and eutrophic phosphate compounds, and their low concentration of ionic species, which prevents issues with sludge formation. The corrosion performance of the coatings is dependent on the substrate material and substrate chemistry. Optimal conversion parameters (composition, pH, immersion time, temperature and stirring) should be determined for each system individually. The possibility of using the same coatings on different substrates (multi-metal coatings on mixed metal components) is advantageous for industrial applications and future work should focus on this issue, as optimization of bath and deposition parameters is needed. Moreover, although studies have been carried out on optimization of conversion bath parameters, further studies would be beneficial, especially in terms of bath composition and subsequent coating composition and its corrosion performance. A large variety of performance was observed for Ti/Zr conversion coatings, ranging from relatively poor to excellent. Results obtained on Al alloys and Zn coated steels are already advanced, but more work is needed on steels and Mg alloys. Zr and Ti conversion coatings primarily offer barrier protection, and upgrading the functionality of these coatings by incorporation of self-healing agents like Ce and V would be advantageous. The incorporation of Cr(III) compounds seems beneficial, but recent evidence that the presence of Cr(III) results in the formation of Cr(VI) compounds could generate environmental concerns, even if the concentrations are much smaller than for CCCs. Some studies reported the beneficial effect of bath additives and chemical post-treatments, so further studies should concentrate on these subjects.

For the coatings that contain organic components, the interactions between organic and inorganic phases should be investigated

in more detail. The chemical reactions of the organic phase affect the polymerization and condensation reactions within the coating and consequently affect the coating structure as well as the chemical composition of the surface. The latter determines the subsequent adhesion of the organic topcoat, which is very important for performance in industrial applications.

The assessment of a conversion pre-treatment on a substrate with no additional coating does not provide an indication of how the pre-treatment will perform as a part of a full coating system. Further understanding of the interactions between conversion coatings and organic topcoats is required to improve both adhesion and cathodic delamination properties. Introduction of methods capable to analyze the interactions in situ would be beneficial.


In summary, conversion coatings based on Ti and/or Zr have great potential for further development and offer many interesting research issues from both fundamental and applied points of view.

### Acknowledgments

The collaboration between Jožef Stefan Institute and The Ohio University, Fontana Corrosion Center, was financed by Slovenian Research Agency as bilateral project between Slovenia and USA "Corrosion protection of technologically important materials using environmentally-friendly coatings" ID BI-US/15-16-006. The authors thank Ph.D. students U. Tiringier and G. Šekularac for technical help during manuscript preparation.

### ORCID

I. Milošev  <https://orcid.org/0000-0002-7633-9954>

G. S. Frankel  <https://orcid.org/0000-0003-0573-3548>

### References

1. R. W. Revie, *Uhlig's Corrosion Handbook*, p. 1284, John Wiley & Sons, (2011).
2. J. K. Hawkins, H. S. Isaacs, S. M. Heald, J. Tranquada, G. E. Thompson, and G. C. Wood, *Corros. Sci.*, **27**, 391 (1987).
3. S. W. M. Chung, J. Robinson, G. E. Thompson, G. C. Wood, and H. S. Isaacs, *Philos. Mag. Part B*, **63**, 557 (1991).
4. J. S. Wainright, O. J. Murphy, and M. R. Antonio, *Corros. Sci.*, **33**, 281 (1992).
5. J. Zhao, G. Frankel, and R. L. McCreery, *J. Electrochem. Soc.*, **145**, 2258 (1998).
6. S. Adhikari, K. A. Unocic, Y. Zhai, G. S. Frankel, and John Zimmerman, *Electrochimica Acta*, **56**, 1912 (2011).
7. <https://monographs.iarc.fr/ENG/Monographs/vol100C/>.
8. [http://europa.eu/rapid/press-release\\_IP-10-1465\\_en.htm?locale=en](http://europa.eu/rapid/press-release_IP-10-1465_en.htm?locale=en).
9. <https://www.osha.gov/>.
10. <http://www.waterworld.com/articles/iww/print/volume-14/issue-6/features/adapting-to-more-stringent-cooling-water-discharge-guidelines.html>.
11. S. Jegannathan, T. S. N. Sankara Narayanan, K. Ravichandran, and S. Rajeswari, *Surf. Coat. Technol.*, **200**, 6014 (2006).
12. M. Bethencourt, F. J. Botana, M. J. Cano, M. Marcos, J. M. Sánchez-Amaya, and L. González-Rovira, *Corros. Sci.*, **51**, 518 (2009).
13. M. Kendig, S. Jeanjaquet, R. Addison, and J. Waldrop, *Surf. Coat. Technol.*, **140**, 58 (2001).
14. J. W. Bibber, *Met. Finish.*, **99**, 15 (2001).
15. M. W. Kendig and R. G. Buchheit, *Corrosion*, **59**, 379 (2003).
16. T. G. Harvey, *Corros. Eng. Sci. Technol.*, **48**, 248 (2013).
17. M. Forsyth, M. Seter, M. Y. Tan, and B. Hinton, *Corros. Eng. Sci. Technol.*, **49**, 130 (2014).
18. Y. Ota and T. Kojima, *Kobelco Technol. Rev.*, **35**, 61 (2017).
19. U. Karmaschek, A. Roland, H. Vennschott, and H. Wennemann, (1996) <http://www.google.com/patents/US5584946>.
20. D. Y. Dollman, S. E. Dolan, and L. E. Steinbrecher, (1996) <http://www.google.com/patents/US5534082>.
21. C. E. Tomlinson, (1998) <http://www.google.com/patents/US5759244>.
22. M. Matsukawa, K. Makino, and T. Shimakura, (2004) <http://www.google.com/patents/US20040187967>.
23. B. H. Goodreau, J. Liu, E. Kopic, and M. Febraro, (2009) <http://www.google.com/patents/US20090232996>.
24. V. Donald, E. Kopic, B. Goodreau, and A. Bobadilla, (2012) <http://www.google.com/patents/US20120301739>.
25. D. R. Vonk, E. Kopic, and M. L. Sienkowski, (2013) <http://www.google.com/patents/US20130266819>.
26. E. Kopic, B. H. Goodreau, A. Bobadilla, and M. Febraro, (2017) <http://www.freepatentsonline.com/y2017/0137947.html>.
27. T. R. Giles, B. H. Goodreau, W. E. Fristad, J. Kroemer, and M. Frank, *SAE Int. J. Mater. Manuf.*, **1**, 575 (2008).
28. T. R. Giles, D. R. Vonk, and S.-L. Favero, in, p. 172, *Henkel Corporation*, Sao Paulo, Brazil (2012) [www.abts.org.br/biblioteca-anais-ebrats-download.asp?arquivo=36.pdf](http://www.abts.org.br/biblioteca-anais-ebrats-download.asp?arquivo=36.pdf).
29. I. Paloumpa, A. Yfantis, P. Hoffmann, Y. Burkov, D. Yfantis, and D. Schmeißer, *Surf. Coat. Technol.*, **180–181**, 308 (2004).
30. Y. Liu, Y. Yang, C. Zhang, T. Zhang, B. Yu, G. Meng, Y. Shao, F. Wang, and L. Liua, *J. Electrochem. Soc.*, **163**, C576 (2016).
31. S. Le Manchét, D. Verchère, and J. Landoulsi, *Thin Solid Films*, **520**, 2009 (2012).
32. J. Winiarski, J. Masalski, and B. Szczygieł, *Surf. Coat. Technol.*, **236**, 252 (2013).
33. M. Oki, *J. Appl. Sci. Environ. Manag.*, **11**(2), 187 (2007).
34. C. Stromberg, P. Thissen, I. Klueppel, N. Fink, and G. Grundmeier, *Electrochimica Acta*, **52**, 804 (2006).
35. L. Zhu, F. Yang, and N. Ding, *Surf. Coat. Technol.*, **201**, 7829 (2007).
36. X. Chen, G. Li, J. Lian, and Q. Jiang, *Appl. Surf. Sci.*, **255**, 2322 (2008).
37. X. Chen, G. Li, J. Lian, and Q. Jiang, *Surf. Coat. Technol.*, **204**, 736 (2009).
38. S. Verdier, S. Delalande, N. van der Laak, J. Metson, and F. Dalard, *Surf. Interface Anal.*, **37**, 509 (2005).
39. H. Ardelean, I. Frateur, S. Zanna, A. Atrons, and P. Marcus, *Corros. Sci.*, **51**, 3030 (2009).
40. D. Chidambaram, C. R. Clayton, and G. P. Halada, *Electrochimica Acta*, **51**, 2862 (2006).
41. P. D. Deck and D. W. Reichgott, *Met. Fin.*, **90**, 29 (1992).
42. P. D. Deck, M. Moon, and R. J. Sujdak, *Prog. Org. Coat.*, **34**, 39 (1998).
43. P. Puomi, H. M. Fagerholm, J. B. Rosenholm, and R. Sipilä, *Surf. Coat. Technol.*, **115**, 79 (1999).
44. M. A. Smit, J. A. Hunter, J. D. B. Sharman, G. M. Scamans, and J. M. Sykes, *Corros. Sci.*, **45**, 1903 (2003).
45. M. A. Smit, J. A. Hunter, J. D. B. Sharman, G. M. Scamans, and J. M. Sykes, *Corros. Sci.*, **46**, 1713 (2004).
46. L. Wang, B. Peng, X. Guo, W. Ding, and Y. Chen, *Chem. Commun.*, 1565 (2009).
47. M. Niknahad, S. Moradian, and S. M. Mirabedini, *Corros. Sci.*, **52**, 1948 (2010).
48. Y. Guan, J. G. Liu, and C. W. Yan, and others, *Int J Electrochem Sci.*, **6**, 4853 (2011).
49. F. O. George, P. Skeldon, and G. E. Thompson, *Corros. Sci.*, **65**, 231 (2012).
50. A. Yi, W. Li, J. Du, and S. Mu, *Appl. Surf. Sci.*, **258**, 5960 (2012).
51. P. Taheri, K. Lill, J. H. W. de Wit, J. M. C. Mol, and H. Terryn, *J. Phys. Chem. C*, **116**, 8426 (2012).
52. T. Lostak, S. Krebs, A. Maljusch, T. Gothe, M. Giza, M. Kimpel, J. Flock, and S. Schulz, *Electrochimica Acta*, **112**, 14 (2013).
53. X. Zhong, X. Wu, Y. Jia, and Y. Liu, *Appl. Surf. Sci.*, **280**, 489 (2013).
54. R. Posner, N. Fink, M. Wolpers, and G. Grundmeier, *Surf. Coat. Technol.*, **228**, 286 (2013).
55. T. Lostak, A. Maljusch, B. Klink, S. Krebs, M. Kimpel, J. Flock, and S. Schulz, and W. Schuhmann, *Electrochimica Acta*, **137**, 65 (2014).
56. A. Ghanbari and M. M. Attar, *Surf. Coat. Technol.*, **246**, 26 (2014).
57. R. Mohammad Hosseini, A. A. Sarabi, H. Eivaz Mohammadloo, and M. Sarayloo, *Surf. Coat. Technol.*, **258**, 437 (2014).
58. S. S. Golru, M. M. Attar, and B. Ramezanzadeh, *J. Ind. Eng. Chem.*, **24**, 233 (2015).
59. Z. Xi, W. Li, S. Mu, J. Du, Y. Yang, and P. Tang, *Prog. Org. Coat.*, **87**, 61 (2015).
60. A. Yi, J. Du, J. Wang, S. Mu, G. Zhang, and W. Li, *Surf. Coat. Technol.*, **276**, 239 (2015).
61. A. Yi, W. Li, J. Du, and S. Mu, *Surf. Interface Anal.*, **47**, 863 (2015).
62. P. Taheri, P. Laha, H. Terryn, and J. M. C. Mol, *Appl. Surf. Sci.*, **356**, 837 (2015).
63. N. W. Khun and G. S. Frankel, *Mater. Corros.*, **66**, 1215 (2015).
64. S. Sharifi Golru, M. M. Attar, and B. Ramezanzadeh, *Appl. Surf. Sci.*, **345**, 360 (2015).
65. A. Salmasifar, A. A. Sarabi, and H. Eivaz Mohammadloo, *Corros. Eng. Sci. Technol.*, **50**, 372 (2015).
66. H. Eivaz Mohammadloo and A. A. Sarabi, *Prog. Org. Coat.*, **101**, 391 (2016).
67. H. R. Asemani, P. Ahmadi, A. A. Sarabi, and H. Eivaz Mohammadloo, *Prog. Org. Coat.*, **94**, 18 (2016).
68. H. R. Asemani, A. A. Sarabi, H. E. Mohammadloo, and M. Sarayloo, *J. Coat. Technol. Res.*, **13**, 883 (2016).
69. W. Zhu, W. Li, S. Mu, Y. Yang, and X. Zuo, *Appl. Surf. Sci.*, **384**, 333 (2016).
70. W. Zhu, W. Li, S. Mu, N. Fu, and Z. Liao, *Appl. Surf. Sci.*, **405**, 157 (2017).
71. S. Verdier, N. van der Laak, F. Dalard, J. Metson, and S. Delalande, *Surf. Coat. Technol.*, **200**, 2955 (2006).
72. S. Le Manchét, J. Landoulsi, C. Richard, and D. Verchère, *Surf. Coat. Technol.*, **205**, 475 (2010).
73. H. Eivaz Mohammadloo and A. A. Sarabi, *Corrosion*, **72**, 791 (2016).
74. P. Santa Coloma, U. Izaguirre, Y. Belaustegi, J. B. Jorcin, F. J. Cano, and N. Lapena, *Appl. Surf. Sci.*, **345**, 24 (2015).
75. C. Cai, X.-Q. Liu, X. Tan, G.-D. Li, H. Wang, J.-M. Li, and J.-F. Li, *Mater. Corros.*, **68**, 338 (2017).
76. Y. Yu, Q. Zhang, J. Xie, and J. Y. Lee, *Nat. Commun.*, **4**, 1454 (2013).
77. L. Fedrizzi, F. Deflorian, and P. L. Bonora, *Electrochimica Acta*, **42**, 969 (1997).
78. J. S. Costa, R. D. Agnoli, and J. Z. Ferreira, *Tecnol. Em Metal. Mater. E Min.*, **12**, 167 (2015).
79. B. Szczygieł, J. Winiarski, and W. Tylus, *Mater. Chem. Phys.*, **129**, 1126 (2011).
80. A. S. Hamdy and M. Farahat, *Surf. Coat. Technol.*, **204**, 2834 (2010).
81. G. Yoganandan, K. Pradeep Premkumar, and J. N. Balaraju, *Surf. Coat. Technol.*, **270**, 249 (2015).
82. H. Eivaz Mohammadloo and A. A. Sarabi, *Appl. Surf. Sci.*, **387**, 252 (2016).
83. H. Bubert, H. Puderbach, H. Pulm, and W. A. Roland, *Fresenius J. Anal. Chem.*, **333**, 304 (1989).

84. P. Smith and C. Miller, (2007) <http://oai.dtic.mil/oai/oai?verb=getRecord&metadataPrefix=html&identifier=ADA464887>.
85. J. Cerezo, I. Vandendael, R. Posner, K. Lill, J. H. W. de Wit, J. M. C. Mol, and H. Terryn, *Surf. Coat. Technol.*, **236**, 284 (2013).
86. J. Cerezo, P. Taheri, I. Vandendael, R. Posner, K. Lill, J. H. W. de Wit, J. M. C. Mol, and H. Terryn, *Surf. Coat. Technol.*, **254**, 277 (2014).
87. J. Cerezo, I. Vandendael, R. Posner, J. H. W. de Wit, J. M. C. Mol, and H. Terryn, *Appl. Surf. Sci.*, **366**, 339 (2016).
88. A. Sarfraz, R. Posner, M. M. Lange, K. Lill, and A. Erbe, *J. Electrochem. Soc.*, **161**, C509 (2014).
89. D. Peng, J. Wu, X. Yan, X. Du, Y. Yan, and X. Li, *J. Coat. Technol. Res.*, **13**, 837 (2016).
90. P. Laha, T. Schram, and H. Terryn, *Surf. Interface Anal.*, **34**, 677 (2002).
91. G. Gusmano, G. Montesperelli, M. Rapone, G. Padeletti, A. Cusmà, S. Kaciulis, A. Mezzi, and R. Di Maggio, *Surf. Coat. Technol.*, **201**, 5822 (2007).
92. L. Li, A. L. Desouza, and G. M. Swain, *Analyst*, **138**, 4398 (2013).
93. N. W. Khun, G. S. Frankel, and J. Zimmerman, *Corrosion*, **69**, 259 (2013).
94. O. Lunder, C. Simensen, Y. Yu, and K. Nisancioglu, *Surf. Coat. Technol.*, **184**, 278 (2004).
95. O. Lunder, F. Lapique, B. Johnsen, and K. Nisancioglu, *Int. J. Adhes. Adhes.*, **24**, 107 (2004).
96. H. Eivaz Mohammadloo, A. A. Sarabi, A. A. Sabbagh Alvani, H. Sameie, and R. Salimi, *Surf. Coat. Technol.*, **206**, 4132 (2012).
97. H. E. Mohammadloo, A. A. Sarabi, A. A. S. Alvani, R. Salimi, and H. Sameie, *Mater. Corros.*, **64**, 535 (2013).
98. E. Ramanathan and S. Balasubramanian, *Prog. Org. Coat.*, **93**, 68 (2016).
99. M. Sababi, H. Terryn, and J. M. C. Mol, *Prog. Org. Coat.*, **105**, 29 (2017).
100. Z. P. Cano, J. R. Kish, and J. R. McDermid, in *Materials Science and Technology (MS&T) 2013 Conference Proceedings*, Warrendale, PA 15086–7514 USA, 1591 (2013).
101. M. P. Brady, W. J. Joost, and C. David Warren, *Corrosion*, **73**, 452 (2016).
102. I. Schoukens, I. Vandendael, J. De Strycker, A. A. Saleh, H. Terryn, and I. De Graeve, *Surf. Coat. Technol.*, **235**, 628 (2013).
103. N. W. Khun and G. S. Frankel, *Corros. Sci.*, **67**, 152 (2013).
104. F. Andreatta, A. Lanzutti, L. Paussa, and L. Fedrizzi, *Prog. Org. Coat.*, **77**, 2107 (2014).
105. J. H. Nordlien, J. C. Walmsley, H. Østerberg, and K. Nisancioglu, *Surf. Coat. Technol.*, **153**, 72 (2002).
106. L. Li, B. W. Whitman, and G. M. Swain, *J. Electrochem. Soc.*, **162**, C279 (2015).
107. F. Andreatta, A. Turco, I. de Graeve, H. Terryn, J. H. W. de Wit, and L. Fedrizzi, *Surf. Coat. Technol.*, **201**, 7668 (2007).
108. J. Cerezo, R. Posner, I. Vandendael, J. H. W. de Wit, H. Terryn, and J. M. C. Mol, *Mater. Corros.*, **67**, 361 (2016).
109. H. Ardelean, I. Frateur, and P. Marcus, *Corros. Sci.*, **50**, 1907 (2008).
110. X.-F. Xia, Y.-Y. Gu, and S.-A. Xu, *Appl. Surf. Sci.*, **419**, 447 (2017).
111. J.-W. Brouwer, J. Krömer, S. Cornen, M. Frank, N. Heischkamp, and F.-A. Czika, (2009) <http://www.google.ch/patents/WO2009115504A1>.
112. L. Li, B. W. Whitman, C. A. Munson, R. Estrada, C. A. Matzdorf, and G. M. Swain, *J. Electrochem. Soc.*, **163**, C718 (2016).
113. V. Saarimaa, E. Kauppinen, A. Markkula, J. Juhanaja, B.-J. Skrifvars, and P. Steen, *Surf. Coat. Technol.*, **206**, 4173 (2012).
114. H. Eivaz Mohammadloo, A. A. Sarabi, R. Mohammad Hosseini, M. Sarayloo, H. Sameie, and R. Salimi, *Prog. Org. Coat.*, **77**, 322 (2014).
115. M. Morcillo, S. Feliu, J. Simancas, J. M. Bastidas, J. C. Galvan, S. Feliu Jr., and E. M. Almeida, *Corrosion*, **48**, 1032 (1992).
116. S. Feliu, J. C. Galvana, S. Feliu Jr., J. M. Bastidas, J. S. Imancas, M. Morcillo, and E. M. Almeida, *Corros. Sci.*, **35**, 1351 (1993).
117. G. Matamala, W. Smeltzer, and G. Droguett, *Corrosion*, **50**, 270 (1994).
118. E. Kusmirek and E. Chrzescijanska, *Mater. Corros.*, **66**, 169 (2015).
119. N. W. Khun, S. Adhikari, Y. Y. Li, G. S. Frankel, J. McGee, T. Smith, B. Bammel, and J. Zimmerman, *Corrosion*, **73**, 339 (2016).
120. Y. Guo and G. S. Frankel, *Corrosion*, **68**, 045002 (2012).
121. L. Li, D. Y. Kim, and G. M. Swain, *J. Electrochem. Soc. JES*, **159**, C326 (2012).
122. J. Qi, L. Gao, Y. Liu, B. Liu, T. Hashimoto, Z. Wang, and G. E. Thompson, *J. Electrochem. Soc. JES*, **164**, C442 (2017).
123. R. Moore and B. Dunham, *Met. Finish.*, **106**, 46 (2008).
124. L. Fedrizzi, A. Bianchi, F. Deflorian, S. Rossi, and P. L. Bonora, *Electrochimica Acta*, **47**, 2159 (2002).
125. N. W. Khun and G. S. Frankel, *Corrosion*, **71**, 277 (2015).
126. K. Ogle, S. Morel, and N. Meddah, *Corros. Sci.*, **47**, 2034 (2005).
127. M. P. Brady, D. N. Leonard, H. M. Meyer III, J. K. Thomson, K. A. Unocic, H. H. Elsentriecy, G.-L. Song, K. Kitchen, and B. Davis, *Surf. Coat. Technol.*, **294**, 164 (2016).
128. A. F. Carreira, A. M. Pereira, E. P. Vaz, A. M. Cabral, T. Ghidini, L. Pigliaru, and T. Rohr, *J. Coat. Technol. Res.*, **1** (2017).
129. M. Stratmann, *Corrosion*, **61**, 1115 (2005).
130. H. Leidheiser, W. Wang, and L. Igetoft, *Prog. Org. Coat.*, **11**, 19 (1983).
131. G. Grundmeier, W. Schmidt, and M. Stratmann, *Electrochimica Acta*, **45**, 2515 (2000).
132. M. A. Hernandez, F. Galliano, and D. Landolt, *Corros. Sci.*, **46**, 2281 (2004).
133. W. Furbeth and M. Stratmann, *Corros. Sci.*, **43**, 207 (2001).
134. B. C. Rincon Troconis and G. S. Frankel, *Surf. Coat. Technol.*, **236**, 531 (2013).
135. L. I. Fockaert, P. Taheri, S. T. Abrahami, B. Boelen, H. Terryn, and J. M. C. Mol, *Appl. Surf. Sci.*, **423**, 817 (2017).
136. S. Wang, C. Liu, and F. Shan, *Acta Metall. Sin. Engl. Lett.*, **22**, 161 (2009).
137. S. Yu, R. Zhang, Y. Tang, Y. Ma, and W. Du, *J. Nanomater.*, **2013**, 1 (2013).
138. A. Ghanbari and M. M. Attar, *Appl. Surf. Sci.*, **316**, 429 (2014).
139. M. A. Smit, J. M. Sykes, J. A. Hunter, J. D. B. Sharman, and G. M. Scamans, *Surf. Eng.*, **15**, 407 (1999).
140. J. Simancas, D. de la Fuente, B. Chico, L. Madueno, F. Camon, M. C. Blanco, and M. Morcillo, *Prog. Org. Coat.*, **76**, 1833 (2013).